ACS OMEGA

Open Access

http://pubs.acs.org/journal/acsodf

Review

Advancements and Perspectives in Optical Biosensors

Shahriar Mostufa, Bahareh Rezaei, Stefano Ciannella, Parsa Yari, Jenifer Gómez-Pastora, Rui He, and Kai Wu*

Cite This: *ACS Omega* 2024, 9, 24181−24202

Read Online

ACCESS | Metrics & More | Article Recommendations

ABSTRACT: Optical biosensors exhibit immense potential, offering extraordinary possibilities for biosensing due to their high sensitivity, reusability, and ultrafast sensing capabilities. This review provides a concise overview of optical biosensors, encompassing various platforms, operational mechanisms, and underlying physics, and it summarizes recent advancements in the field. Special attention is given to plasmonic biosensors and metasurface-based biosensors, emphasizing their significant performance in bioassays and, thus, their increasing attraction in biosensing research, positioning them as excellent candidates for lab-on-chip and point-of-care devices. For plasmonic biosensors, we emphasize surface plasmon resonance (SPR) and its subcategories, along with localized surface plasmon resonance (LSPR) devices and surface enhance Raman spectroscopy (SERS), highlighting their ability to perform diverse bioassays. Additionally, we discuss recently emerged metasurface-based biosensors. Toward the conclusion of this review, we address current challenges, opportunities, and prospects in optical biosensing. Considering the advancements and advantages presented by optical biosensors, it is foreseeable that they will become a robust and widespread platform for early disease diagnostics.

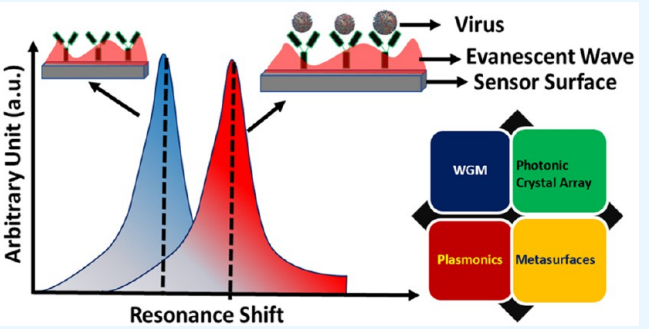

1. INTRODUCTION

Biosensors are devices that can detect and quantify the specific existence of biological substances and molecular compounds from biological samples.[1] Their fundamental part is to convert the molecular recognitions or binding events into physical signals. Among the various approaches to convert biological interactions to physical signals, optical biosensors have attracted significant attention in biosensing research due to their broad sensitivity and wide range of applications.[2] Besides that, optical biosensors offer significant advantages due to their low noise and immunity to electromagnetic interference.[3,4] Optical biosensors represent an essential analytical tool for providing necessary information regarding the bioassay's concentrations, kinetics of binding, and molecular structures. They utilize numerous optical phenomena such as reflection, absorption, fluorescence, scattering transmission, and intensity to classify and quantify the target analytes for quantitative bioassays.[5] Over the past two decades, the optical biosensors based on the analyte refractive index change, such as whispering gallery mode (WGM),[6,7] photonic crystal waveguide cavity resonators,[8,9] surface plasmon resonance (SPR),[10,11] localized surface plasmon resonance (LSPR),[12,13] optical fiber plasmonic coating,[14,15] photonic crystal fibers (PCF),[16,17] and most recently, metasurfaces[18,19] emerged as potential candidates for biomedical use. The optical resonance sensors are susceptible to the surrounding medium, and any changes in the medium caused by the binding events of ligand analytes or the concentrations of analytes can easily be detected without the requirement of complex labels/tags. Unlike magnetic sensors such as giant magnetic resistance (GMR)[20−24] and magnetic tunnel junctions (MTJ)[25,26] sensors, where the target biological substances are tagged with magnetic nanoparticles (MNPs),[22] the optical sensors can detect the real-time refractive index change of analytes in the interaction of the dielectric interface without any labels/tags.[1,27,28]

A critical aspect of identifying and controlling diseases requires highly sensitive, ultrafast, and cost-effective (reusable) diagnostic techniques. The conventional polymerase chain reaction (PCR)[29−31] and enzyme-linked immunosorbent assays (ELISA)[32,33] are powerful tools for detecting diseases but are time-consuming and cost-ineffective.[34] For instance, the ELISA method requires several reagents to interact and create a signal (e.g., incubation steps are time-consuming, and for some pathogens, it is not even realizable). On the other

Received: February 26, 2024
Revised: May 10, 2024
Accepted: May 14, 2024
Published: May 30, 2024

hand, while the PCR method is accurate and robust for detection, it is limited to previously known nucleic acid sequences. Consequently, optical-based biosensors have emerged as a promising alternative for biomolecule detection. The fundamental detection principle of optical biosensors relies on the evanescent wave mechanism—a wave that exponentially decays by penetrating the outer medium of the sensor surface. This mechanism is observed at the interface between the medium and the surfaces of the photonic sensors. The biomolecular interaction, represented by changes in the refractive index in bioassays, influences the properties of the evanescent wave. As the evanescent wave is exponentially decaying, it exists only at a minimal distance from the sensor surface. Thus, most of the optical biosensors rely on the induced change in the effective refractive index in the evanescent area region. As a result, optimizing the structure of optical sensors is crucial for achieving peak performance, necessitating significant effective refractive index changes.[35] This optimization involves careful consideration of factors such as operating wavelength, sensor structural parameters, sensor surface biofunctionalization, and the resolutions of the optical spectrum analyzer (OSA) device. Each of these elements is a prerequisite that collectively contributes to the detection sensitivity of optical biosensors. Therefore, a sophisticated design is essential to enhance the biosensor's detection capability. In optical biosensing, some essential sensor parameters are sensitivity, specificity, signal-to-noise ratio, detection limit, etc. The sensitivity is calculated based on the change of the resonance condition, such as for the wavelength-based interrogation method; the wavelength sensitivity is defined as the ratio of the resonance wavelength shifts due to the change in the concentration of bioassays.[36] Similarly, for the angular interrogation method, the sensitivity is calculated as the ratio of resonance angle changes with the concentration change in the bioassays.[28] The detection limit is the minimum amount of concentration required to detect a change in the resonance condition. Specificity is defined as the capability of the sensor to produce the response only in the presence of a specific target molecule.[37] The signal-to-noise ratio (SNR) is defined as the ratio of the signal power to noise power over a spectral bandwidth. The SNR considers the noise from all sources, such as thermal, electrical, optical, and even environmental.

Optical biosensors based on resonance have demonstrated tremendous advancements and are actively investigated by the research community as they offer high sensitivity down to single biomolecule interactions without labeling.[38−42] For instance, the organophosphorus (OP) pesticide by optofluidic ring resonator[43] and microRNAs (miRNAs)[44] are detectable by label-free optical biosensors. Furthermore, various surface modifications, biofunctionalization, and immobilization methods are necessary for specific bioassays and the achievement of the full potential of optical sensing devices.[35] Various biomolecules can be used as receptors, and several types of methods exist for the biofunctionalization of the sensor surface,[45,46] such as physical absorption,[47] covalent binding,[48] and noncovalent interactions.[49] Moreover, advancements in microfabrication and microfluidic channel technologies have facilitated the reduction in the size of optical sensors. This progress positions them as highly promising point-of-care (POC) devices for the early detection of diseases and medical diagnostics.[50] Additionally, optical sensors have all the features present to be effectively used as POC devices, such as label-free detections, reusability, low cost and high sensitivity, and notably, multiple analyte detection (i.e., multiplexing). Likewise, the miniaturized lab-on-a-chip (LOC)[51,52] optical biosensor devices, incorporating all functionalities from sample preparation to signal generation, are portable and user-friendly, catering to a broad user base.

This review provides a comprehensive overview of the sensing principles, recent advancements, and applications of optical resonance biosensors across various platforms, showcasing their efficacy in detecting diverse bioassays. The illustration of the optical biosensors covered in this review is showcased in Figure 1, and the application of these sensors in several bioassays and their performance are summarized in Table 1 at the end of this review. Our focus has primarily been on the different kinds of optical biosensors and how they have evolved for their use in biomedical applications. Section 2 provides an overview of WGM biosensing applications and recent developments. Section 3 discusses various photonic crystal cavities and their potential applications in biosensing. In Section 4, we reviewed prism-coupled SPR sensors, optical fibers with surface plasmonic coating sensors, photonic crystal fiber sensors, LSPR biosensors, and surface-enhanced Raman spectroscopy (SERS). Furthermore, in Section 5, we delve into

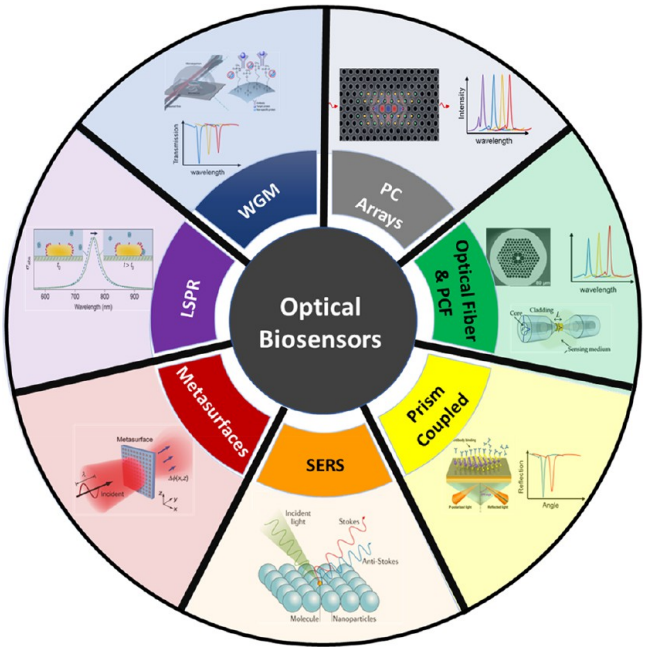

Figure 1. Schematic drawing overviews of different types of optical biosensors covered in this review. Whispering gallery mode (WGM) reprinted from ref 53 under a Creative Commons Attribution 4.0 International License, 2015. 2D photonic crystal array reprinted with permission from ref 54. Copyright 2019 AIP Publishing. Prism coupled SPR angular modulation-based biosensor reprinted from ref 55 under a Creative Commons Attribution 4.0 International License, 2016. Photonic crystal fiber (PCF) based biosensing reprinted with permission from ref 56. Copyright 2020 Optical Society of America. Optical fibers with plasmonic coating biosensing reprinted from ref 57 under a Creative Commons Attribution 3.0 International License, 2011. Surface enhance Raman spectroscopy (SERS) reprinted with permission from ref 58. Copyright 2021 Springer Nature Limited. Metasurfaces based optical biosensors reprinted with permission from ref 59. Copyright 2016 WILEY-VCH Verlag GmbH & Co. KGaA, Weinheim.

https://doi.org/10.1021/acsomega.4c01872
ACS Omega 2024, 9, 24181−24202

Table 1. Summary of Optical Biosensors on Numerous Platforms Reported in the Literature

Technology Platform	Optical Structure	Materials	Modulation Technique	Bioassays analyte (Molar mass)	Detection limit	Sensitivity	Year[ref]
Whispering Gallery Mode (WGM)	Microsphere	Silica	Wavelength	Single influenza A virus (InfA) virions (5.2×10^{-16} g)	-	-	2008[63]
	Microtoroid	-		Single protein−protein and receptor−ligand (~15.2 kDa)	2.5 nm (nanoparticle radius)	-	2016[40]
	Microsphere	Au-NPs/GO_x		Glucose (180.15 g/mol)	_	-	2020[156]
	Microcavity	Polymer		Horseradish peroxidase (HRP) (~40 kDa)	0.3 ng/mL	-	2020[157]
				vascular endothelial growth factor (VEGF) (~40 kDa)	17.8 fg/mL		
	WGM fiber	-		Streptavidin (~60 kDa)	3 nM	0.008 nm/nM	2022[158]
	Ring microcavity	Hollow-core microbottle cavity (HC-MBC) functionalized		label-free DNA	260 aM		2023[159]
	Plasmon coupled micro rings	GaN/AuNPs		Urine pH value	10^{-9} M	-	2023[160]
Photonic Crystal Array Waveguide	Line defect-M shaped	Si	Wavelength	Simulation analysis (RI)	_	570 nm/RIU	2011[161]
	Nanocavity	SOI		Human IgG molecules	1.5 fg	$2.3 \pm 0.24 \times 10^5$ nm/M	2011[162]
	Nanobeam cavity	SOI		Single polystyrene	14 nm radius (NP)	439 nm/RIU	2015[163]
	Nanohole photonic crystals with plasmonics	Si with gold (Au)		Epstein−Barr nuclear antigen-1 (EBNA-1) antibody	10^{-3} μg/mL	-	2017[164]
	Ring-shaped resonators	silicon rods		Cancer biomarkers	_	308.5 nm/RIU	2023[165]
Plasmonic Resonance	Prism coupled	Prism/gold/borophene/antimonene/SM	Angular	-	4.84×10^{-6} RIU	206.26 deg/RIU	2021[92]
		Au/$PtSe_2$/graphene		Hemoglobin in blood and urine glucose	-	200 deg/RIU	2021[85]
		TiO_2/Au/graphene		Cancer biomarkers	-	292.86 deg/RIU	2022[28]
		Prism/gold/ε-SnSe/gold/graphene/SM		-	-	214 deg/RIU	2022[93]
		Au/Ag/AlN		Urine glucose	-	411 deg/RIU	2023[166]
		Ag/$BiFeO_3$/AgNC/$BiFeO_3$		Water pollution	6.058×10^{-4} RIU	448.1 deg/RIU	2023[167]
		Au/tantalum pentoxide (Ta_2O_5)/antimonene		miRNA	76.91 fM	2.53×10^{-5} deg/(fM).	2024[94]
	Multilayer grating	Silver/gold coated	Wavelength	mouse IgG antibodies	4.12×10^{-5}RIU	356 nm/RIU	20017[168]
		Gold-coated BAF10 grating		Blood glucose	-	2600 nm/RIU	2020[169]
		Gold grating/polydimethylsiloxane		Glucose and industrial solution	-	311.97 nm/RIU	2022[170]
		Ag/TiO_2/ZnO grating		Cancer bioassays	-	12633.57 nm/RIU	2023[86]
	Photonic crystal fiber	Silver coated D shape	Wavelength	Biochemical	-	21,700 nm/RIU	2017[110]
		D shape side polish (Au)		Bovine serum albumin	-	6,328 nm/RIU	2019[171]
		PCF LSPR biosensor (Au nanodisks)		Refractive index	-	500 nm/RIU	2020[172]
		Microchannel (Au/TiO_2)		Refractive index	6.83×10^{-12} RIU^2/nm	121,000 nm/RIU	2021[173]
		MXene between Silica and Gold		Protein, viruses, cancer, and blood cells	1.075×10^{-6} (RIU)	13,000 nm/RIU	2022[174]
	Optical fiber	Ω-Shaped	Wavelength	*Salmonella typhimurium* C-reactive protein	128 CFU/mL	64.582 (a.u.)/RIU	2018[175]
		Au/MoS_2		*E. coli* bacteria	94 CFU/mL	0.6 nm/(1000 CFU/mL)	2019[96]
		Coreless Ti/Au		human immunoglobulin G (HIgG)	0.465 μg/mL	215 nm/(mg/mL)	2019[97]
		hollow core multimodal fiber		DNA hybridization	1 pM	4.04 nm/log(μM)	2022[176]

https://doi.org/10.1021/acsomega.4c01872
ACS Omega 2024, 9, 24181−24202

Table 1. continued

Technology Platform	Optical Structure	Materials	Modulation Technique	Bioassays analyte (Molar mass)	Detection limit	Sensitivity	Year[ref]
		GO/Gold NP/MoS_2NP		Cardiac Troponin I protein	96.26 (ng/mL)	3.4 pm/(ng/mL)	2022[177]
		Silanized ball resonator		CD44 cells concentrations	107 ag/mL (4.7 aM)	-	2022[178]
		gold coated tilted fiber Bragg grating		HER2 (Human Epidermal Growth Factor Receptor-2)	10^{-12} g/mL	-	2023[179]
		Gold nanorods		Acetylcholine	0.45 μg/mL	0.4912 nm/(μg/mL)	2024[180]
Metasurfaces	Double split ring	-	Wavelength	Alpha fetoprotein-Glutamine transferase isozymes II	0.02524 μg/mL	-	2017[151]
	Elliptical zigzag array	-		Mouse IgG	~3 molecules per μm^2	-	2019[181]
	Gradient Au nanorods array	-		Streptavidin−biotin binding	15 nM	-	2019[182]
	nanotrench structures	Al/Ge/Au		L-proline, D-glucose, and sodium chloride, nanoparticles (liposomes)	~1 pg	-	2021[183]
	2D asymmetric microarray	-		extracellular vesicles	204 fM	305 nm/RIU	2021[184]
	Pattern structure Au	-		carcinoem- bryonic antigen (CEA)	0.1 ng/mL	76.5 GHz/RIU	2021[185]
	Split-ring resonator	-		cancer biomarkers CA199 and CA125	0.01 U/mL	65 GHz/RIU	2022[186]
	Nanorod HMM	-		streptavidin	0.14 μg/mL	41,600 nm/RIU	2022[150]
	L corner	Au/SiC		Cancer bioassays	-	3.74 THz/RIU	2023[36]
	double-open square and ring resonator	Metal/SiO_2/Si		MicroRNA (miRNA)	100 aM	5.56 GHz/ $lgC_{miRNA-21}$	2024[187]

https://doi.org/10.1021/acsomega.4c01872
ACS Omega 2024, 9, 24181−24202

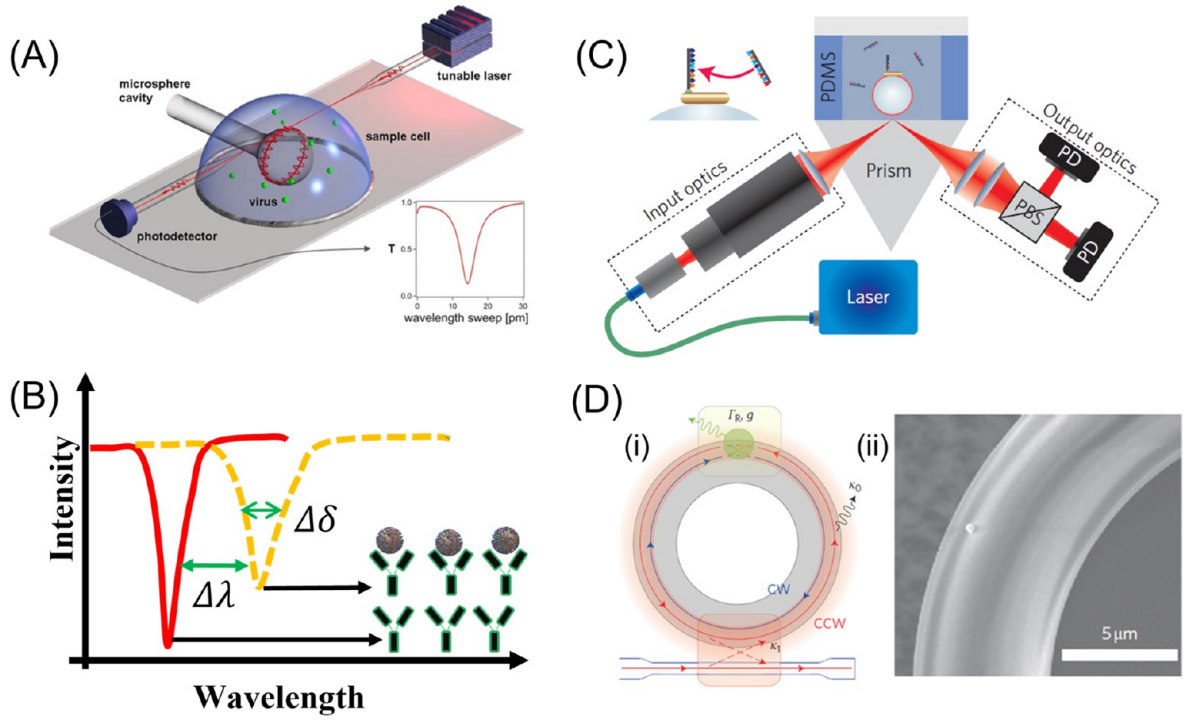

Figure 2. (A) Experimental demonstration of WGM in biosensing. (A) Reprinted with permission from ref 63. Copyright 2008 by The National Academy of Sciences of the USA. (B) Depending on the surface refractive index, the resonance wavelength shifts in the transmission spectrum curve. (C) Enhancing the performance of WGM biosensor with plasmonic nanorods for detecting a single oligonucleotide; for liquid sample, polydimethylsiloxane (PDMS), and for detecting transverse magnetic (TM) and transverse electric (TE) polarization, the photodetector (PD) polarizing beam splitter is employed. (C) Reprinted with permission from ref 66. Copyright 2014 Springer Nature Limited. (D) Deposited nanoparticle (radius 150 nm) onto the microtoroid cavity resonator surface for a mode splitting experiment (i) schematic view, (ii) scanning electrode microscope (SEM) images. (D) Reprinted with permission from ref 68. Copyright 2010 Springer Nature Limited.

the most recent developments and biosensing applications achieved through metasurfaces. Then, in Section 6, we present the current research focus, developments, and challenges of optical biosensors, highlighting the necessary advancements to transform them into effective POC devices.

2. WHISPERING GALLERY MODE (WGM) BIOSENSORS

In 1878, Lord Rayleigh unveiled the whispering gallery phenomenon at St. Paul's Cathedral, showcasing its application in acoustic waves. Subsequently, this phenomenon found resonance in the realm of optics, specifically within micro-optical WGM resonators, where light waves propagate near the resonator boundary.[60] The presence of WGM in the optical resonator is a result of total internal reflection (TIR). The greater the difference in the refractive index between the resonator cavity and its surroundings, the stronger the confinement, leading to a higher observed quality factor (Q). Nevertheless, the propagating wave inside the resonator possesses an evanescent tail that extends beyond the cavity, fostering a coupling between the WGM propagating wave and the environment, which works as a sensing probe for the surrounding medium variations.[61]

The optical resonance condition[61,62] for WGM is denoted as $m\lambda = 2\pi R n_{\text{eff}}$ for one round trip, where the integer number is denoted as m, λ is the light wavelength, R is the radius of the resonator, and n_{eff} is the effective refractive index between the resonator and the environment. Hence, any change in the physical size or the refractive index of the resonator induced by a variation of bioassays or chemical composition of the medium would change the resonance condition in a way such as wavelength shifting, mode splitting, and the line width broadening of the initial condition. This inherent sensitivity to alterations in the external medium makes the WGM sensor an ideal candidate for biosensing applications.

Vollmer et al.[63] demonstrated the exquisite capability of this sensor to detect individual particles of the influenza virus, elucidating their experimental setup in Figure 2(A). When a virion binds to the microresonator surface, there is a resonance wavelength shift obtained by monitoring the output transmission spectrum. Similarly, as illustrated in Figure 2(B), when the immobilized antibodies specifically bind with the analyte on the resonator surface, the resonance shifts due to the refractive index modulation within the surrounding medium.[64] For instance, Quan et al.[65] numerically unveil the peptide thickness growth based on the change in resonance frequency of the WGM sensor. Later, in pursuit of augmenting performance and pushing the limits of detection for WGM sensors, Baaske et al.[66] utilized gold nanorods to enhance the plasmons depicted in Figure 2(C). They also presented the single oligonucleotides (single nucleic acid) detection, which was impossible to detect with only WGM sensors. The plasmonic resonance can enhance the optical signal on the resonator surface as well as the resonance shift due to the binding of an oligonucleotide. In addition, Subramanian et al.[67] employed multiple gold nanorod structures for sensing protein conformational variation.

Furthermore, Zhu et al.[68] reported the detection and sizing of individual particles by using the mode-splitting phenomenon observed in the transmission spectrum of microtoroid

https://doi.org/10.1021/acsomega.4c01872
ACS Omega 2024, 9, 24181−24202

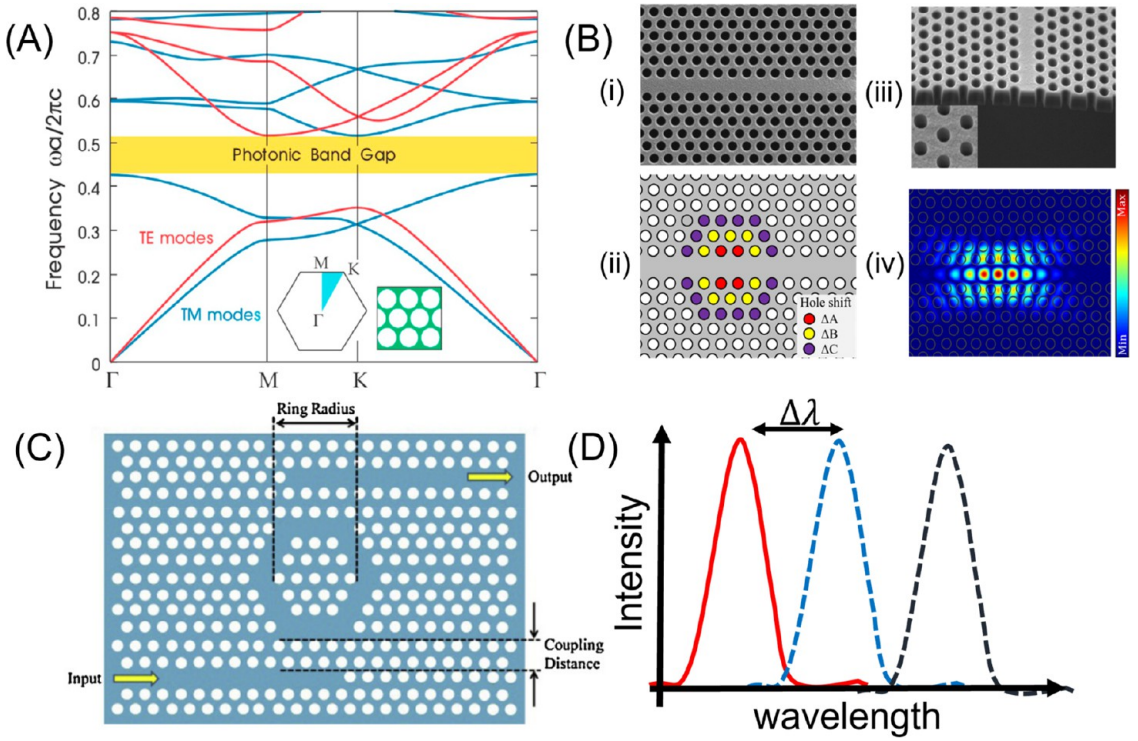

Figure 3. (A) Photonic bands representations where the TE mode is marked with red and the TM mode is marked with blue, and the complete PBG is presented in yellow. (A) Reprinted with permission from ref 82. Copyright 1997 Springer Nature Limited. (B) (i) SEM image of fabricated PhA with line defects, (ii) schematic representation of PhA with line width defects at marked red, yellow, and purple holes; (iii) SEM image of cross-section view showing air hole onto the silicon substrate, (iv) cavity resonance mode numerical results. (B) Reprinted from ref 83 under a Creative Commons Attribution 4.0 International License, 2017. (C) PhA ring cavity. (C) Reprinted with permission from ref 75. Copyright 2015 Elsevier B.V. (D) Presentations of transmission spectrum at output.

structure, as showcased in Figure 2(D). They demonstrated that, given the same frequency, two modes exist in a degenerate state: clockwise (CW) and counterclockwise (CCW). Through examining the presence of degenerate CW and CCW modes, they discovered that mode splitting is caused by the disruption of this degeneracy by nanoparticle scatterers (particles scatter onto the surface of the WGM sensor). Thus, it is also feasible to determine the particle's size using this mode splitting in the transmission spectrum.

Later, Kim et al.[69] extended this exploration on the mode splitting but in the aquatic medium for detecting the target nanoparticle in the water by optimizing the resonator's size and focusing on the quality factor. In an aquatic medium, the *Q*-factor undergoes substantial decreases during the transition from an air medium to a water medium, impacting the resonator due to absorption losses in water. Therefore, a high *Q*-factor in WGM is essential for sensing in aquatic mediums. The sensitivity and quality factor of the WGM sensor depend not only on the resonator's structure but also on material losses, absorption, and the presence of surface scatterers, all of which play a crucial role in its performance. Therefore, in recent years, significant developments have been made by combining the WGM resonators with advanced optical materials. For instance, microresonators fabricated with chalcogenide glass can achieve as high as 5×10^4 *Q*-factor.[70] It is because the chalcogenide glass provides a high linear refractive index (e.g., refractive index around 2−3); so, higher confinement is achieved for having high contrast and reduced radiative losses.[71] Recently, Duan et al.[72] proposed a machine learning (ML) technique that uses neural network algorithms to forecast the outcome and harness the entire transmission signal rather than merely concentrating on monitoring a single mode of the WGM transmission spectrum.

3. 2D PHOTONIC CRYSTAL ARRAY (NANOCAVITY) BIOSENSORS

The photonic crystal structure is a dielectric periodic arrangement that can manipulate light in the optical wavelength scale. It was first proposed by Yablonovitch[73] and John[74] back in 1987, and since then, it has found its way to a wide range of applications in optical sensing.[75,76] This section focuses on the 2D photonic crystal array (PhA) structure and its potential application in optical biosensing. The spatial periodic variation in the refractive index in photonic crystals can limit the transmission of electromagnetic (EM) waves or light in particular frequency bands within their structure. Periodic arrangements lead to the creation of photonic band gaps. The term photonic band gap (PBG) refers to a certain band frequency restriction, as highlighted in Figure 3(A). The PBG is similar to the electronics band gap found in semiconductor materials.[77] PBG, a distinctive feature of PhA structures compared to optical fibers and other waveguides, is rooted in the Bloch theory of solid-state physics. It modulates electromagnetic waves with corresponding wavelengths through Bragg's law. As the light cannot propagate into a certain PBG frequency, this phenomenon is used to make the PhA a waveguide structure by introducing defects and slabs.

As shown in Figure 3(B), a line defect is initially introduced by removing one line from the periodic arrangement of PhA. This allows the light wave to propagate into the structure

https://doi.org/10.1021/acsomega.4c01872
ACS Omega 2024, 9, 24181−24202

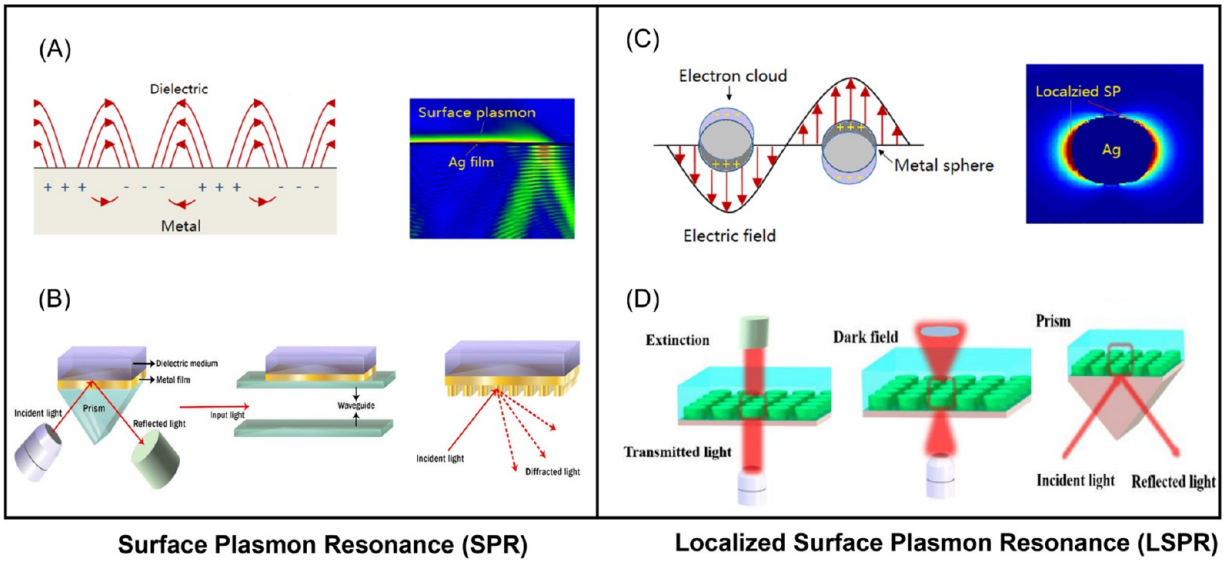

Figure 4. (A) Schematic of surface plasmon polariton (SPP) wave generation using a thin metal layer with the corresponding simulation results (right). (C) The generation of localized surface plasmon resonance (LSPR) in metallic nanostructures along with the simulation outcomes (right). (B) and (D) exhibit the different biosensing methods for exciting SPR and LSPR, respectively. (A) and (C) reprinted with permission from ref 88. Copyright 2012 WILEY-VCH Verlag GmbH & Co. KGaA, Weinheim. (B) Reprinted from ref 89 under a Creative Commons Attribution 4.0 International License, 2022. (D) Reprinted from ref 84 under a Creative Commons Attribution 4.0 International License, 2021.

without loss in the periodic arrangement. The presence of the line defect enables light with a frequency within the PBG range to propagate without losses, as it cannot enter the periodic arrangement due to the band gap. Consequently, the structure becomes a waveguide through the line defect or slab line. However, for biosensing applications, the confinement of evanescent waves is essential. Therefore, an optical cavity is established within the PhA structure to meet this requirement.

As presented in Figure 3(B) (ii), the cavity is formed by altering the diameters of some air holes along the line defect slab, and Figure 3(B) (iv) illustrates the resonance mode within the cavity. Likewise, Zhang et al.[75] present a ring cavity structure in Figure 3(C). Within the cavity region, where samples are either placed or certain air holes are filled with samples, the evanescent wave interacts with the sample material (bioassay refractive index). Depending on the variations in the sample, resonance shifts are observed in the output transmission spectrum, as shown in Figure 3(D).

For instance, Lee et al.[78] demonstrated a PhA structure for detecting a total mass of 2.5 fg bovine serum albumin (BSA) binding with glutaraldehyde. They have experimentally fabricated their device on silicon on insulator (SOI) wafer and coated their sensor surface with various sizes of protein to obtain the resonance shifts, while BSA binds to glutaraldehyde. Similarly, the surface of the PhA immobilized with a specific biotarget capture for a selective biomolecular and wide range of detection was reviewed, as showcased by Inan et al.[76] Scullion et al.[79] presented the detection of a minimum concentration of 15 nM of avidin in an ultracompact-sized cavity of 2.2 μm^2. They first diluted the egg-white lyophilized avidin powder from 100 $\mu g/mL$ to 1 ng/mL in phosphate-buffered saline (PBS) and then injected it into their PhA sensor to monitor the resonance redshifts for all the concentrations. In summary, the cavity region is sensitive to the local area of the defects, and both the cavity region and wavelength in the PhA structure can be tuned by altering the structure.[80] Therefore, it can be used in combination with optofluidic technology for potential biomedical applications.[81]

4. NANOPLASMONIC BIOSENSORS

4.1. Fundamentals of Nanoplasmonics. Plasmonic refers to the oscillation of free electrons triggered by the influence of the excitation of the EM wave (lightwave). This collective oscillation of the electrons exists in the large metallic surface and the localized area of the metallic nanoparticle. For the surface plasmon resonance (SPR), also known as surface plasmon waves (SPW), the plasmonic mode is excited and propagates along the interface of a metal and the dielectric medium (i.e., the sensing medium),[84] as depicted in Figure 4(A). This phenomenon generates an evanescent field that serves as a sensitive probe for biosensing applications, reacting to changes in the surrounding medium. SPR interaction is attainable in several ways, including prism coupling,[85] grating coupling,[86] and waveguide coupling,[87] as illustrated in Figure 4(B).

On the other hand, scenarios where the phenomenon is restricted to subwavelength-sized metallic nanoparticles with specific excitation frequency are known as LSPR, shown in Figure 4(C). LSPR originates from nonpropagating conduction electron waves for the interaction between the EM field and the metal nanosized structure. Upon excitation by light waves, LSPR leads to increased absorption, scattering, and EM field enhancement near the nanoparticle or nanostructure metals.[84] Figure 4(D) exhibits several methods for exciting the LSPR: (i) extinction, (ii) dark field, and (iii) prism. LSPR-based biosensors offer faster assays as samples disperse more rapidly over nanoparticle surfaces compared to metallic thin films, benefiting from enhanced evanescent waves that are generated in LSPR near the metallic nanostructure. In the following sections, we reviewed several SPR and LSPR configurations and their potential applications in biosensing.

4.2. Multilayer Structures (Prism Coupled) Biosensors. In the multilayer angular modulation based SPR

https://doi.org/10.1021/acsomega.4c01872
ACS Omega 2024, 9, 24181−24202

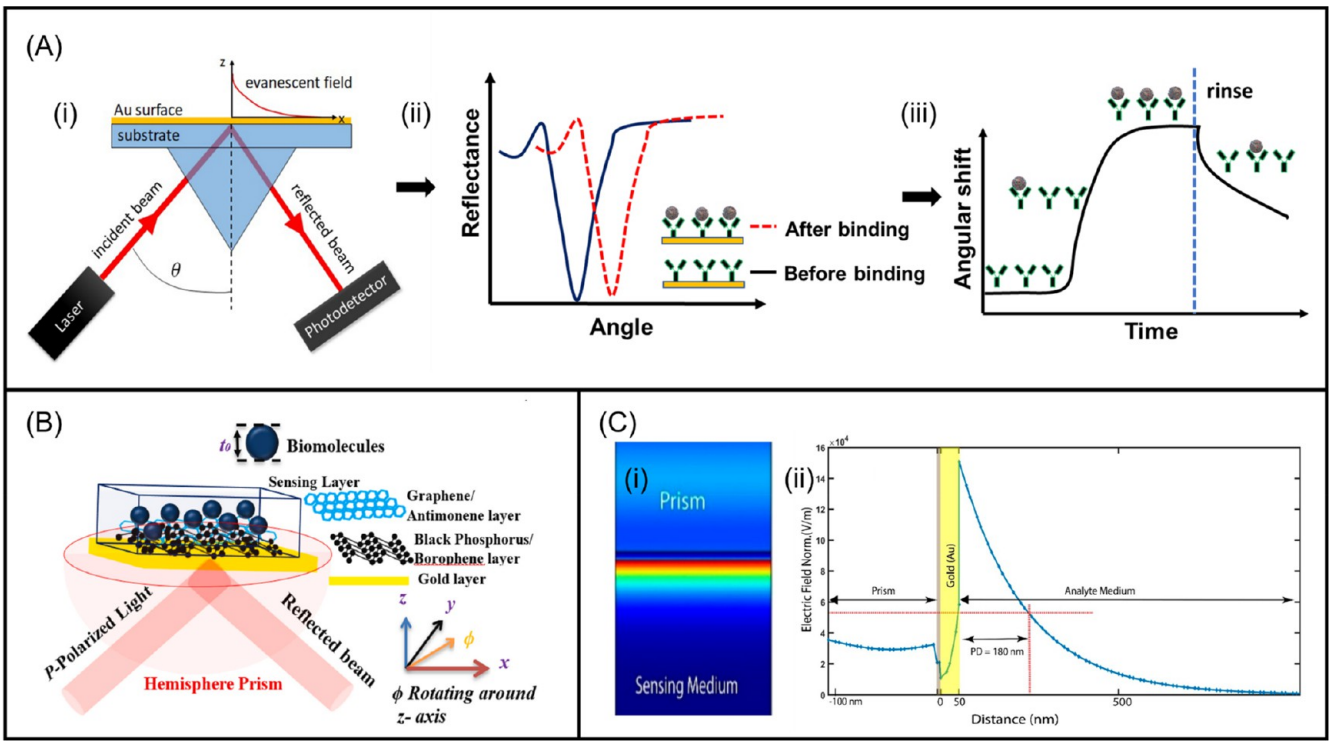

Figure 5. (A) The system architecture of a surface plasmon resonance instrument: device setup showing angle modulation technique (i), resonance angle shift due to binding interaction between the probe ligand and the analyte (ii), real-time sensorgram curve (iii). (A) Reprinted from ref 91 under a Creative Commons Attribution 4.0 International License, 2022. (B) Sensor performance enhancement using the multilayers with 2D materials along with a metallic layer. (B) Reprinted with permission from ref 92. Copyright 2021 Elsevier B.V. (C) FEM simulation results showing field enhancement in the metallic layer (i) and the penetration depth of the evanescent wave from the metal layer (right (ii)). (C) Reprinted from ref 28, under a Creative Commons Attribution 4.0 International License, 2022.

detection approach, the metallic thin film is excited with an optical light wave for generating the surface plasmon polaritons (SPP) (the SPP propagated wave is known as SPW), which propagates along the waveguide interface between metal and dielectric layer. For the propagation of SPW, the wavevector of SPP and the incident light wave must match. Depending on the arrangement of the metal and the dielectric layer, there are two types of multilayer prism-based SPR configurations, the Otto[90] and the Kretschmann[85] configurations. This section is focused on the Kretschmann configuration, a widely utilized arrangement in SPR biosensing.[91]

Figure 5(A) illustrates the biosensing mechanism in the Kretschmann configuration. Initially, a gold thin film is immobilized with a probe ligand, and upon excitation with an optical wave, a resonance curve is obtained. Subsequently, the analyte is introduced, leading to analyte-ligand interactions on the sensor surface. This results in a shift in the resonance angle, as shown in Figure 5(A) (ii). The real-time monitoring of this resonance angle shift, depicted in a sensorgram, provides a representation of binding interactions. The sensor detects changes in the sensing medium using the evanescent wave that extends outside the sensor surface to the sensing medium (existing several nanometers outside the metal layer), as illustrated in Figure 5(C). Additionally, enhanced field distribution has been observed from the finite element method (FEM) analysis results on the gold surface under resonance conditions.[28]

Recent advancements have seen a resurgence in the popularity of prism-based multilayered hybridized SPR refractive index biosensors, particularly through the innovative integration of multilayer configurations and the inclusion of novel 2D material layers. These enhancements, as highlighted in Figure 5(B), contribute significantly to enhancing sensor performance and stability.[92] In 2021, Verma et al.[92] proposed a sophisticated multilayered biosensor incorporating 2D materials capable of detecting DNA/RNA and other biomolecules. The enhanced sensitivity was attributed to the borophene and antimonene layers, with borophene's high electronic density facilitating chemical binding and effective charge transfer and antimonene's delocalized 5s/5p orbitals enhancing biomolecular absorptions. Additionally, Sathya et al.[93] introduced a bimetallic SPR biosensor featuring multilayer 2D materials, where the ε-SnSe (tin selenide) was sandwiched between dual gold layers, followed by graphene for medical, chemical, and biological biomarker identification. Their sensor exhibited a marked increase in sensitivity, about 93.81% higher than traditional sensors without 2D materials, achieving a sensitivity of 214 deg per refractive index unit (deg/RIU). Most recently, Phan et al.[94] demonstrated the detection of miRNA in a concentration range of 0−1000 fM using an Au/tantalum pentoxide (Ta_2O_5)/antimonene layer and reported a sensitivity of 2.53×10^{-5} deg/fM.

4.3. Optical Fiber Plasmonic Biosensors. Fiber optics relies on the total internal reflection (TIR), where a crucial condition is that the refractive index of the core must exceed that of the cladding, and the incident light at the core-cladding boundary surpasses the critical angle (θ_c), following Snell's law:

$$\theta_c = \sin^{-1}(n_2/n_1) \quad (1)$$

https://doi.org/10.1021/acsomega.4c01872
ACS Omega 2024, 9, 24181−24202

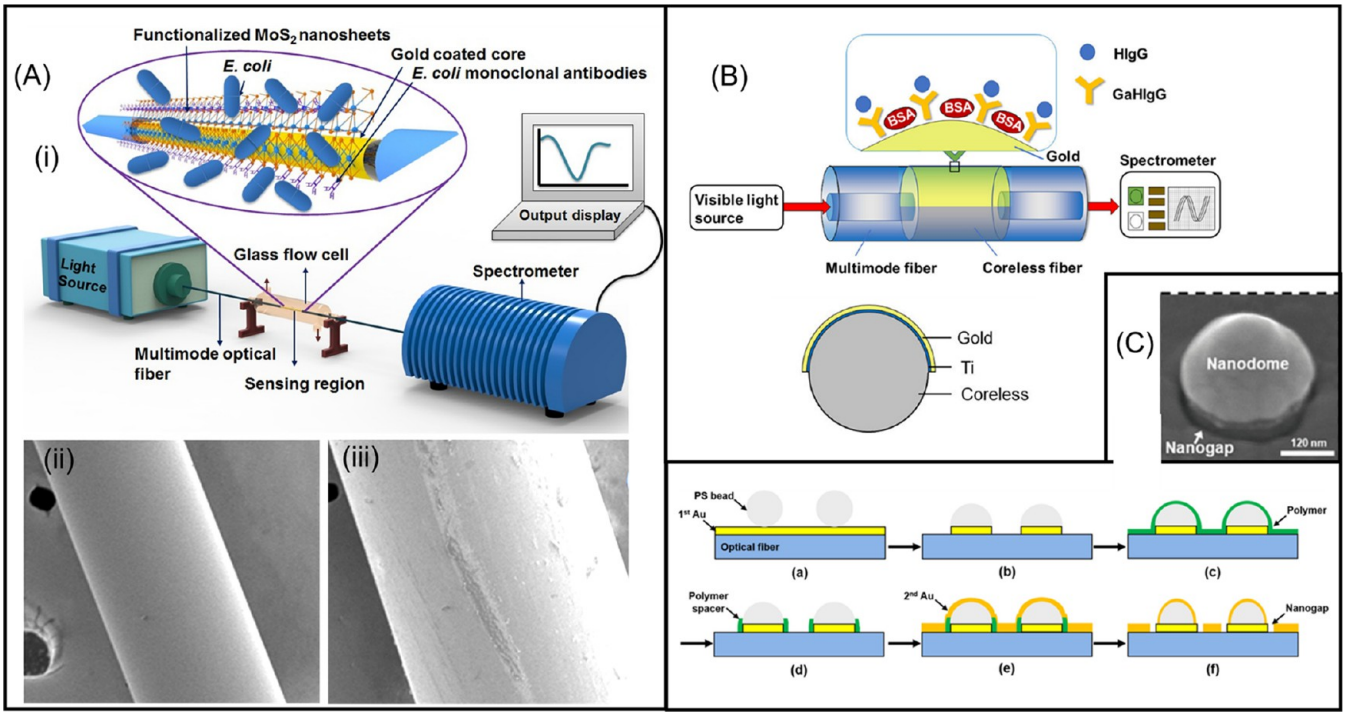

Figure 6. (A) Immunosensor for *E. coli*. detection using fiber optics plasmonic sensors with biofunctionalized MoS_2 nanosheets (i). (ii) and (iii) represent only the Au and Au/MoS_2 optical fiber structure with a field emission scanning electron microscope (FESEM) image, respectively, where functionalized MoS_2 is observable by surface coarseness. (A) Reprinted with permission from ref 96. Copyright 2010 Elsevier B.V. (B) SPR-based optical fiber biosensor with immobilized GaHIgG for detecting HIgG. (B) Reprinted with permission from ref 97. Copyright 2019 IOP Publishing Ltd. (C) The SEM image and the fabrication of dome array with nanogaps (DANG) for optical fiber-based plasmonic biosensing. (C) Reprinted with permission from ref 98. Copyright 2022 American Chemical Society.

where n_1 and n_2 represent the refractive indices of the core and cladding, respectively. While propagating inside the optical fiber, the majority of the light stays inside the core, and only a few, termed evanescent waves, go outside to the cladding region. The penetration depth (d_p) of the evanescent wave can be determined as follows:[95]

$$d_p = \lambda/\pi\sqrt{n_{co}^2 \sin^2\theta - n_{cl}^2} \quad (2)$$

where the incident wavelength is λ, and the angle of incidence at the core-cladding interface is denoted by θ, while n_{co} and n_{cl} signify the refractive indices of the core and the cladding, respectively.

Therefore, for sensing purposes, it is essential to expose the evanescent wave to the metal-dielectric layer to enhance the SPP. The excitations of SPP can be achieved by modifying some parts of the cladding layer with plasmonic material, as depicted in Figure 6(A,B). Following the metal layer, the sensing medium (dielectric layer) is utilized for biosensing purposes. Under resonance conditions, the wave vector of the incident light aligns with that of SPP. Consequently, any variations in the sensing medium during resonance conditions result in changes in the resonance, enabling the detection of analytes.

Several plasmonics fiber optics-based immunosensors have recently been proposed, exhibiting extraordinary performance. For instance, Kaushik et al.[96] proposed an *Escherichia coli* (*E. coli.*) rapid detection using the optical fiber sensor coated with Au/immobilized molybdenum disulfide (MoS_2) materials shown in Figure 6(A). The functionalization of this 2D nanomaterial (MoS_2), immobilized with the monoclonal antibodies, achieved a detection limit of 94 CFU/mL for selective detection of *E. coli* bacteria. Similarly, Lang et al.[97] proposed a multimodal coreless fiber optics-based biosensor coated with Ti/Au for the selective detection of human immunoglobulin G (HIgG). They immobilized goat antihuman immunoglobulin G (GaHIgG) on the sensor surface for the specific detection of HIgG. The proposed sensor achieved a detection limit of 0.465 μg/mL and a sensitivity of 215 nm/(mg/mL), as depicted in Figure 6(B). Most recently, Kim et al.[98] showed the nanogap dome using the Au for an optical fiber-based plasmonic sensor, illustrated in Figure 6(C), achieving the detection limit of 38 fg/mL for the antibody–antigen interactions of thyroglobulin.

4.4. Photonic Crystal Fibers (PCF) Biosensors. Over the last 20 years, photonic crystal fibers (PCFs) have garnered significant research interest due to their superior optical characteristics, which are essential in various emerging technological fields.[87,99,100] Integrating air holes within the fiber structure broadens the spectrum of waveguide parameters, facilitating distinct guiding mechanisms. PCFs are broadly categorized into two types based on their guiding mechanisms: (i) index-guiding PCFs, which operate through modified TIR,[101] similar to traditional fibers, and (ii) photonic bandgap fibers (PBG)-PCFs, which confine light within a low-index solid, hollow core,[102] allowing only specific light wavelengths to pass through. The unique optical properties of PCFs are attributed to their porous structure, which is defined by three main elements: the PCF material, the structural array, and the functional materials (surface coating materials) used in the PCF. These factors collectively contribute to the PCFs' potential in sensor development and other device applications. Photonic crystals revealed their applications in various

https://doi.org/10.1021/acsomega.4c01872
ACS Omega 2024, 9, 24181−24202

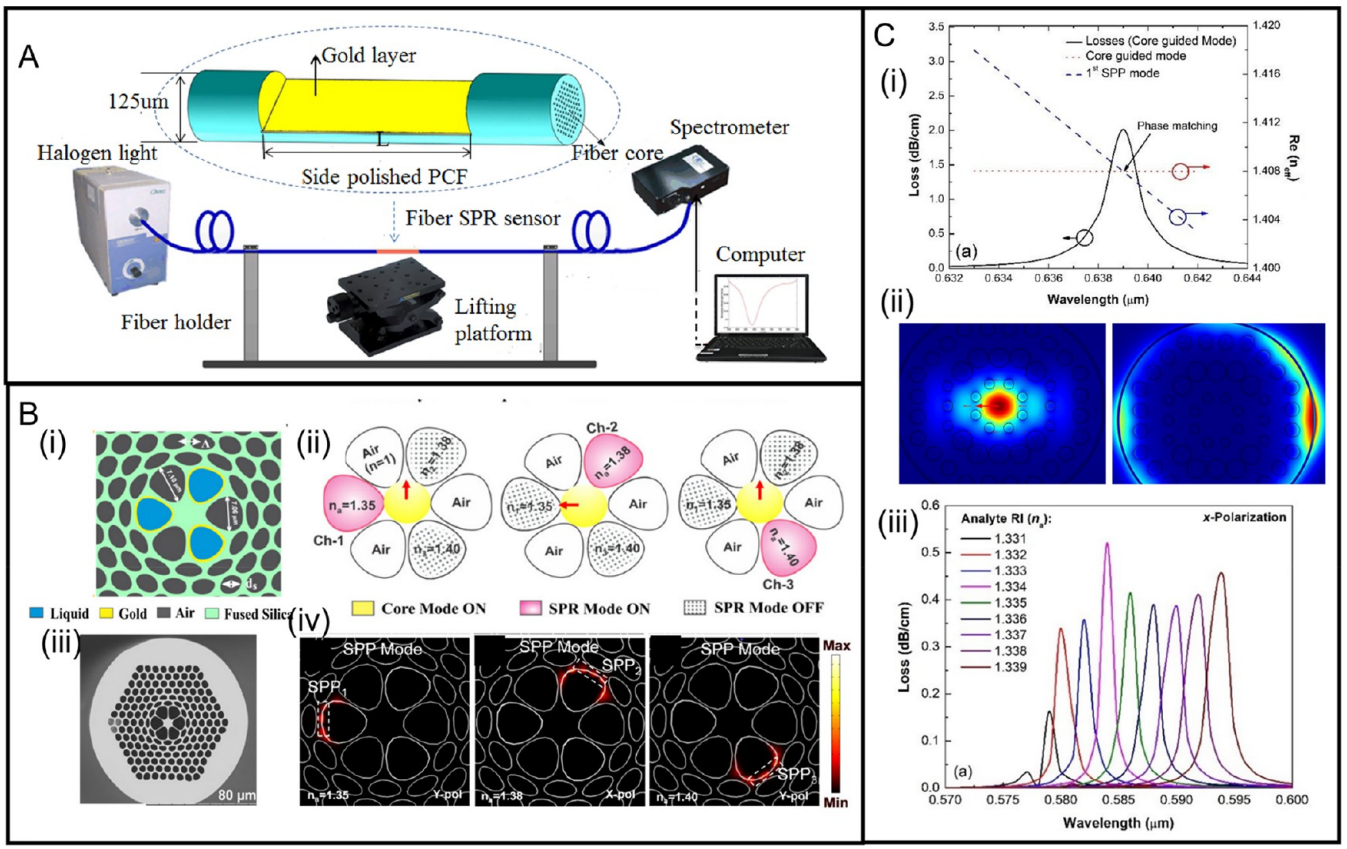

Figure 7. (A) D-shaped PCF real-time measurement system schematic setup. (A) Reprinted with permission from ref 110. Copyright 2017 Optical Society of America. (B) Multiplex PCF: (i) schematic drawing, (ii) different channels for flowing microfluidic analyte, (iii) SEM image, and (iv) the plasmonic excitation. (B) Reprinted with permission from ref 56. Copyright 2020 Optical Society of America. (C) Graphene-based PCF (i) confinement loss (ii) FEM numerical results for core (left) and plasmonic mode (right) (iii) Alteration shifting of confinement loss (resonance peaks) as a function of the target analyte. (C) Reprinted from ref 111. Under a Creative Commons Attribution 4.0 International License, 2021.

promising areas, including tunable fiber polarization filters,[103] PCF lasers,[104] high-efficiency polarizers,[105] and PCF sensors.[100]

The SPR-based PCFs operate on the principle of phase-matching conditions of the SPP model with the guided propagation mode. This phenomenon, depicted in Figure 7(C) (i), is commonly referred to as the resonance condition. From the FEM analysis, the core mode and the SPP mode can be observed, as shown in Figure 7(C) (ii). Similarly, the PCFs SPR is sensitive to the medium RI, and based on the medium RI or the sensing medium variation, the confinement loss shifts (the resonance conditions for SPP and guided light matching), as presented in Figure 7(C) (iii). The fundamental sensing setup, encompassing all instruments from the optical source to the OSA for the PCFs-based devices for biosensing, is shown in Figure 7(A).

There is a significant amount of literature on PCFs-based SPR biosensors reporting on bioassay detection. For instance, Pseudomonas bacteria detection using circular PCF was demonstrated by Jahan et al.,[106] who reported a 20,000 nm/RIU wavelength shift sensitivity. Similarly, Ahmed et al.[107] introduced a PCF design that was coated with Au and magnesium fluoride (MgF_2) and obtained a remarkable sensitivity of 27,958.49 nm/RIU. In 2022, Shakya et al.[108] incorporated titanium dioxide (TiO_2) in their PCF design, creating a robust bond between the metal and the analyte layer. Haider et al.[56] demonstrated grapefruit-shaped PCF for detecting multiple analytes at the same time, as shown in Figure 7(B). Here, three channels were filled with different analytes, and SPP was excited about different sensing wavelengths, as shown in Figure 7(B) (ii, iv). Hence, the versatility of PCFs can be enhanced by modifying parameters like hole size, arrangement, spacing, and shape. Current research focuses on altering PCF shapes, aligning PCFs with standard optical fibers, and utilizing sensitization materials to augment PCF properties. Recognizing these advancements and innovations paves the way for identifying potential trends and challenges in the forthcoming years.[109]

4.5. Localized Surface Plasmon Resonance (LSPR) Biosensors. Among plasmonic biosensors, the LSPR-based biosensors stand out as the most common example of evanescent field-based detection. Like SPR, this evanescent wave is generated by the oscillation of electrons at the interface of the metal nanostructure and dielectric layer. Notably, in conventional plasmonic sensors, the penetration distance of the evanescent wave is around 200−400 nm, as illustrated in Figure 8(A), which is larger than that of most bioassays.[13] Consequently, conventional biosensors generate a large evanescent wave, resulting in limited interaction with light and biomolecules. This limitation has been addressed by recent advances in nanophotonic (LSPR) structures. Nanoplasmonic structures can confine light near their surfaces to dimensions down to tens of nanometers. This confinement creates a strong EM field near the structures, enhancing the performance of molecular fingerprint and bioassay sensing because of strong evanescent field excitations.[112]

https://doi.org/10.1021/acsomega.4c01872
ACS Omega 2024, 9, 24181−24202

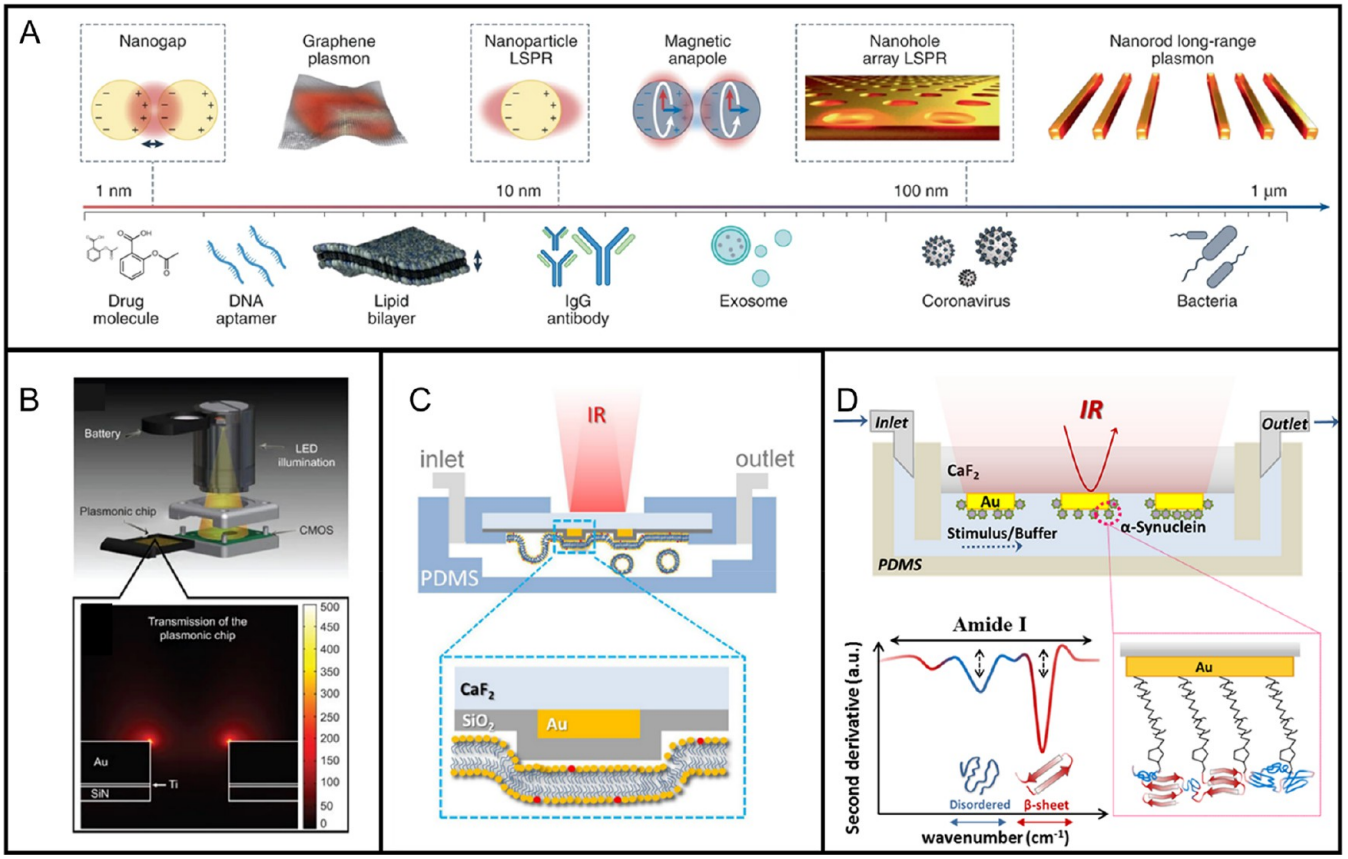

Figure 8. (A) Common bioassays concerning the evanescent wave decay length for numerous nanoplasmonic structures. (A) Reprinted with permission from ref 13. Copyright 2022, Springer Nature Limited. (B) Plasmonic microarrays for an on-chip sensing platform and field enhancement in Au nanoholes with Finite-Difference Time-Domain (FDTD) simulations. (B) Reprinted from ref 118 under the Creative Commons Attribution-NonCommercial-No Derivative Works 3.0 Unported License. (C) The experimental schematic drawing of the fluid chamber for measuring Texas Red DHPE and DOPC which is presented by red and yellow headgroups of phospholipid bioassays. (C) Reprinted with permission from ref 113. Copyright 2016 American Chemical Society. (D) The real-time measurement of the mid-IR range gold nanoantenna array immobilized with proteins (α-synuclein) with different secondary structures (top) and the spectrum exhibits the signature of amide I where the β-sheet component is marked with red color while the blue represents randomly disordered conformation (bottom). (D) Reprinted with permission from ref 114. Copyright 2018 American Chemical Society.

For instance, Limaj et al.[113] presented real-time lipid membrane monitoring with an IR plasmonic sensor having high field enhancements. Their proposed biosensor can detect the formation kinetics and vibrational fingerprints of the lipid molecules in the aqueous medium, as shown in Figure 8(C). The vesicle of lipids was prepared by mixing the Texas Red DHPE (1,2-dihexadecanoyl-*sn*-glycero-3-phos-phoe-thanol-amine) and DOPC (1,2-dioleoyl-*sn*-glycero-3-phosphocholine) with chloroform. Etezadi et al.[114] proposed an enhanced plasmonic nanoantenna and, for the first time, demonstrated the real-time observation of β-sheets due to conformational change in the α-synuclein protein monolayer under various conditions, as shown in Figure 8(D). The protein's monolayer secondary structural dynamics were observed by analyzing the fingerprint of amide I. The conformational variations dynamics of proteins were triggered by environment modulation. Similarly, Adato et al.[115] also demonstrated the protein vibrations using a nanoantenna array. Furthermore, Yanik et al.[116] demonstrated the Fano resonance phenomenon (the asymmetric line shape of resonance curves occurs by coupling subradiant narrow line width modes with super radiant broad line width modes) for monitoring the monolayer of the proteins. Interestingly, Hao et al.[117] presented that by breaking the structural symmetry, the Fano resonance can be excited by directly coupling between the higher order mode and the dipolar mode of the ring cavity and disk, respectively. Cetin et al.[118] presented an on-chip hand-held portable plasmonic microarray with lens biosensing platforms shown in Figure 8(B). The large-scale plasmonic microarray design is integrated into a single device, which enables the same sensor array to be multiplexed and digitally imaged. Li et al.[119] demonstrated the real-time identification of cell-secreted substances in the live cell with the plasmonic nanohole arrays.

Yanik et al.[34] presented the specific detection of intact viruses with plasmonic sensors by dividing the sensor surface into two parts: one functional with antibodies and one unfunctionalized serving as a reference, as showcased in Figure 9(A). The antibody-immobilized portion of the sensor captured the virus, leading to a resonance shift when the biological fluid containing the virus passed over its surface. In contrast, the reference unfunctionalized sensor did not exhibit any resonance changes in contact with the pathogen (vesicular stomatitis virus (VSV)). Additionally, they showcased the detection of a pseudotyped Ebola (PT-Ebola) by immobilizing the Ebola glycoprotein on the sensor chip.

In addition, Zijlstra et al.[121] showed the real-time detection of single molecules by coating the Au nanorod with biotin receptors without any surface amplifications and observed the

https://doi.org/10.1021/acsomega.4c01872
ACS Omega 2024, 9, 24181−24202

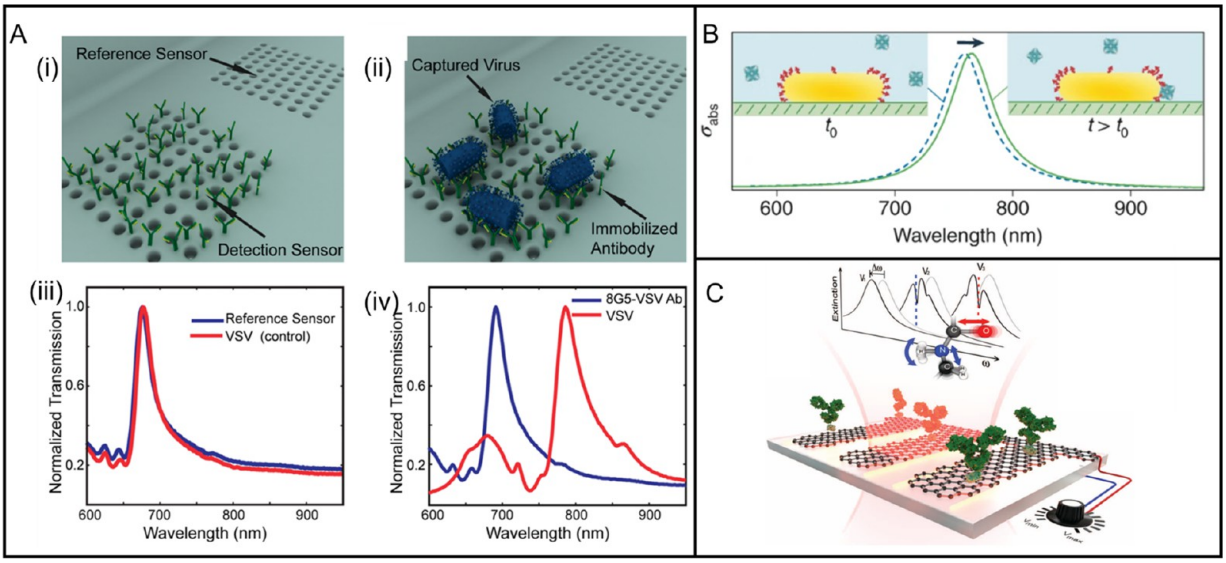

Figure 9. (A) Schematic drawing of nanoplasmonic optofluidic biosensors. (i) The detection sensor contains immobilized antibodies on the sensor surface, and the reference sensor is unfunctionalized. (ii) The antibody on the detection sensor captures the vesicular stomatitis virus (VSV). (iii) For the reference sensor, which is not functionalized, there is no shift in the resonance observed. (iv) The functionalized sensor exhibits a shift in the resonance curve, demonstrating the selective detection of VSV at 10^9 PFU/mL. (A) Reprinted with permission from ref 34. Copyright 2010 American Chemical Society. (B) Biotin functionalized gold nanorod for detecting the conjugates of streptavidin-R-phycoerythrin by real-time binding. (B) Reprinted with permission from ref 121. Copyright 2012 Springer Nature Limited. (C) Mid-IR biosensor with tunable graphene for protein sensing using the molecular vibration with resonance shifting. (C) Reprinted with permission from ref 120. Copyright 2015 American Association for the Advancement of Science.

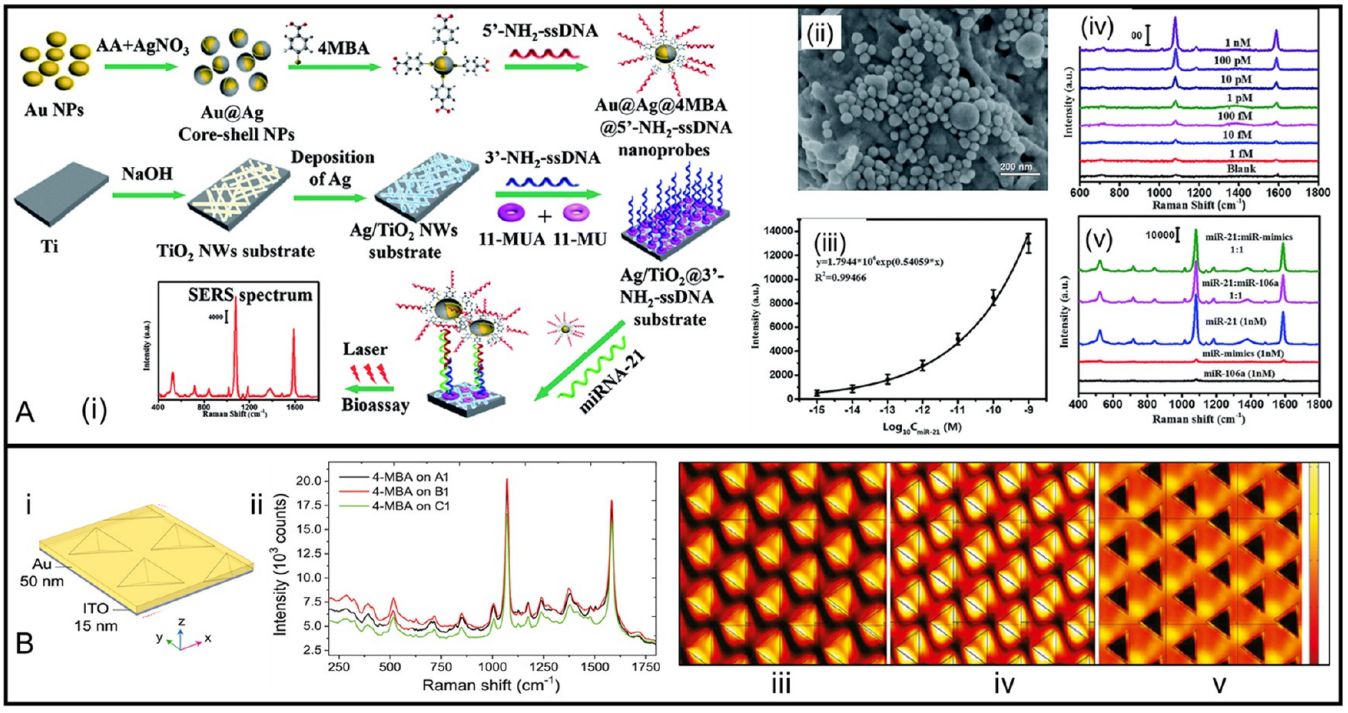

Figure 10. (A) (i) SERS schematics of sandwich bioassays where Au@Ag@4MBA-NH_2-ssDNA probes and substrate were used as the silver NPs-decorated titanium dioxide nanowire (Ag/TiO_2 NWs); (ii) SEM images of sandwich bioassays; (iii–iv) the intensity change due to the concentration of the different concentrations of miRNA-21; (v) at the same concentration of 1 nM, the SERS spectrum of miR-mimics, miR-106a, miRNA-21, and a concentration ratio of 1:1 with their mixture solutions. (A) Reprinted from ref 125 under the Attribution-NonCommercial 3.0 Unported (CC BY-NC 3.0). (B) (i) unit cell structure of Au nanopyramid array SERS substrate; (ii) SERS spectrum for 4-mercaptobenzoic acid (4-MBA) probe on the Au nanopyramid structure for different substrate structure parameters configurations of A1, B1, and C1; and near-field enhancement maps ($|E|/E_0$) for these three different structure configurations of the nanopyramid array in (iii), (iv) and (v) respectively. (B) Reprinted with permission from ref 124. Copyright 2021 American Chemical Society.

plasmonic resonance shifts, as depicted in Figure 9(B). Rodrigo et al.[120] demonstrated the fingerprinting of protein molecules with molecular dimensions of <10 nm and quantitative analysis using a mid-IR tunable graphene-based

https://doi.org/10.1021/acsomega.4c01872
ACS Omega 2024, 9, 24181−24202

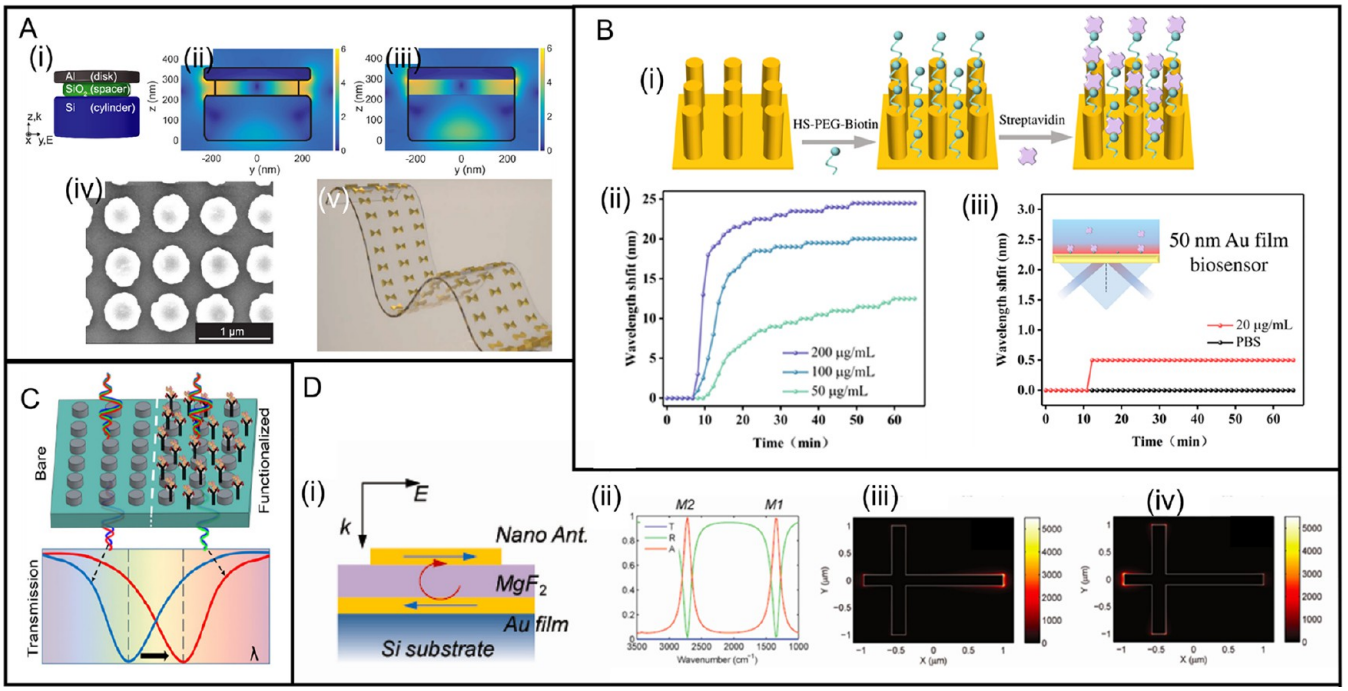

Figure 11. (A) (i) Hybrid metal Al/insulator (SiO_2) structure (ii) with and (iii) without undercut. (iv) SEM top view image. (A) (i–iv) reprinted with permission from ref 134. Copyright 2020 American Chemical Society. (v) Metamaterials printed on a flexible substrate. (A) (v) reprinted with permission from ref 154. Copyright 2011 WILEY-VCH Verlag GmbH & Co. KGaA, Weinheim. (B) The diagram of the biofunctionalization process of Au nanorod hyperbolic metamaterials (NHMMs) biosensors (i) and the sensorgram is shown in (ii–iii) and in the inset showing the overall structure of the sensor setup. (B) Reprinted with permission from ref 150. Copyright 2022 Chinese Laser Press. (C) The metasurface before immobilized without the target ligand and after the ligand analyte binding showing a shift in the resonance spectrum dip. (C) Reprinted with permission from ref 37. Copyright 2022 American Chemical Society. (D) Structure of Au and insulator MgF_2 for unsymmetric cross-shape structure (i), the absorption of the dual-band shown in (ii) and the (iii–iv) electric field intensity for two resonance peaks. (D) Reprinted with permission from ref 153. Copyright 2012 American Chemical Society.

biosensor (see Figure 9(C)). The incident light wave on the graphene surface intensified the interaction with the surface proteins. The narrow resonance peak was generated by light being absorbed by protein biomolecules, and the shift occurred based on the vibrational bands of the proteins. Notably, graphene's LSPR near-field distribution in the mid-IR band exhibits a tighter field confinement than Au.

4.6. Surface Enhanced Raman Spectroscopy (SERS). Surface Enhance Raman scattering (SERS) was first reported in 1974 on pyridine in the silver electrode.[122] Since then, the SERS has gained much interest in research because the use of noble metals (gold, silver, and copper) can certainly enhance electromagnetic fields. Moreover, SERS has some advantages compared to fluorescent-based immunoassays in terms of stability and multiplexed detection.[123] Generally, two major techniques are used for SERS-based detection: one is the label-free approach, and another one is the indirect approach with Raman reported labeled. For instance, in the direct label-free detection method, the SERS signal is obtained using the metallic nanoparticles or the metallic nanoparticles as SERS substrates for specific proteins. Meanwhile, for the indirect method, the Raman-reported molecule is linked with the target protein, and a SERS signal is obtained. For example, Palermo et al.[124] demonstrated the Au pyramid nanohole array structures for enhancing the signal of SERS biosensing, depicted in Figure 10(B). They have showcased that the SERS spectrum intensity changes for the 4-mercaptobenzoic acid (4-MBA) probe depending on the structural parameters of these pyramids. Similarly, Peng et al.[125] presented SERS-based sandwich bioassays using the Au@Ag core–shell and Ag/TiO_2 nanowire substrate for miRNA-21 exhibiting the low limit of detection of 0.75 fM illustrated in Figure 10(A). Also, from Figure 10(A) (iii) and (iv), it can be observed that depending on the change of concentration, the intensity of the SERS changes. Furthermore, Rippa et al.[126] presented a plasmonics octupolar framework of the Au film structure where the SERS enhancement factor achieved 9×10^7 and detected the bacterial toxin. Finally, Wang et al.[127] showcased a multiplexed approach SERS for detecting the prostate-specific antigen (PSA) and α-fetoprotein (AFP) in the human serum by using the SiO_2@Ag immune probes and gold-film hemisphere array (Au-FHA) immune substrate. Their SERS signal can detect the lowest detection concentration of 3.38 and 4.87 fg/mL for PSA and AFP, respectively.

5. METASURFACE-BASED BIOSENSORS

Metasurfaces have recently emerged as one of the most potent biosensing platforms.[128,129] Their exceptional light-matter interaction and little optical power loss have enabled them to possess unique characteristics and be capable of exotic optical sensing properties. In optical biosensing, using metasurfaces to confine light into the nanoscale results in the generation of EM hotspots, enabling the detection of a wide range of bioassays. The foundation of metasurfaces is typically composed of dielectric insulator materials and plasmonic materials such as Au, Ag, and Al.

In plasmonic sensing techniques, the intrinsic losses of the metals cause limitations in detections, which can be overcome

https://doi.org/10.1021/acsomega.4c01872
ACS Omega 2024, 9, 24181–24202

with metasurfaces by using an insulator layer having a low optical loss and high refractive index.[18] The resonance in the metasurfaces is mainly based on the Mie type resonance, where the resonance wavelength and the effective refractive index both depend on the geometric structure,[130,131] and the feature size (unit cell size of metasurfaces) is much smaller compared to the incident light wavelength. This proximity gives rise to the oscillation of displacement currents, manifesting electric and magnetic resonances simultaneously, whereas, in plasmonic sensing, the magnetic fields are very weak. The near field hotspots' Mie scattering results in the engagement with the bioassays in the vicinity of the resonator. By optimizing the metasurface design for a specific application, resonators can be made sensitive to the response of the surrounding medium. Binding interactions involving the target analyte in the medium change the refractive index, which can be easily detected by measuring changes in the resonance conditions. Commercial numerical software packages such as CST Studio Suite[132] and COMSOL Multiphysics[36] are mainly used to observe electric and magnetic field augmentation during resonance conditions.

Karawdeniya et al.[37] exhibited the improvement of a metasurface-based sensor sensitivity by surface functionalization and surface texturing, as illustrated in Figure 11(C). Although metasurfaces have shown tremendous sensitivity and versatility in many branches of optical sensing, bare metasurfaces inherently lack target specificity. Therefore, surface modification methods allow metasurfaces to selectively capture specific bioassays by enabling them to choose particular analytes. Surface modification can be achieved through covalent, noncovalent, and hybrid methods.

Bi et al.[133] employed magnetic control in conjunction with the metasurface biosensor to improve performance in identifying the SARS-CoV-2 spike protein. They linked the antibody (Ab) to the surface of Au nanoparticles first and then to the magnetic nanoparticles (MNPs) (Ab-Au@Fe_3O_4) to enable the magnetic controls. The researchers observed an increase in sensitivity when an external magnetic field was applied. In the absence of the field, particles exhibited Brownian movements, dispersing randomly. However, with the presence of the external magnetic field, the particles congregated at a specific spot and became controllable within the slit zone. This controlled gathering of particles in the presence of the magnetic field contributed to enhanced sensitivity in the sensing system. Similarly, Ray et al.[134] demonstrated the sensitivity improvement of 245 nm/RIU using the undercut in the insulator layer shown in Figure 11(A) (i–iv). The electric field enhancement for the undercut is clearly outside the structure, whereas for having no undercut, it is buried inside the structure's dielectric spacer layer. Thus, the electric field outside the structure enhances the interaction with the medium (e.g., bioassays present in the medium), resulting in sensitivity enhancements.

Metamaterials are getting much attention, especially when it comes to operating in the THz frequency spectrum. For instance, O'Hara et al.[135] used a terahertz time-domain spectroscopy (THz-TDS) approach for a split ring resonator (SRR) metamaterial structure and, for the first time, showcased the transmission resonance shifting effects for THz sensing applications. Similarly, on SRR-designed metamaterials, Singh et al.[136] investigated the impact of geometrical structural gap orientation, and Chiam et al.[137] reported enhancement of the sensitivity and dynamic tuning by the influence of the aspect ratio and the substrate thickness. Gu et al.[138] also showed resonance behavior on flexible and straightforward self-aligned photolithography fabrication based on double-layered close-ring pair terahertz metamaterials. Furthermore, Tian et al.[139] presented the plasmonic hole array of superconductors to gain active control over the thermal and resonance frequency of the THz transmission. They fabricated the unit cell using the material yttrium barium copper oxide hole array on the sapphire substrate and measured the thermal response from room temperature 297 K to 51.4 K and showcased that sharp resonance can be achieved at lower temperatures by cooling the superconductor hole arrays.

Saleh et al.[140] designed a metamaterial asymmetric split resonator for sensing glucose levels with concentrations from 41 to 312 mg/dL, which covers hypoglycemia normal and hyperglycemia conditions with a reporting sensitivity of 438 kHz/(mg/dL). Similarly, Chen et al.[141] showcased the detection of methanol using THz sensing by multimodal resonances in the terahertz regime by breaking the structural symmetry of dual-wire structures. Again, Xu et al.[142] demonstrated a microfluidic integrated dual torus toroidal metamaterial THZ structure with a sensitivity of 124.3 GHz per refractive index. Sreekanth et al.[143] presented the excitations of Brewster modes using a hyperbolic metamaterials (HMMs) structure comprising alternating TiN layers and phase change materials and achieved a sensitivity of about 1.5 $\times 10^{-4}$ RIU deg^{-1}. Also, the confinement of the EM radiation in the subwavelength cavity is important to achieve light-matter interactions. The radiative and the nonradiative losses define the quality factor (Q) of the confined mode at resonance. For instance, Gupta et al.[144] demonstrated an "I" shaped THz metamaterial design capable of confining huge EM waves in low mode volume, giving rise to a significant quality factor per effective volume. Also, Lim et al.[145] reviewed the Fano resonant metamaterial structures, focusing on the latest developments of high-Q. Sajeev et al.[146] used the THz-TDS approach for identifying 2D reduced graphene oxide (r-GO) using the dipole cavities (hole array), showcasing 12 GHz/μm sensitivity for the porous r-GO film. Usually, the change from graphene oxide (GO) to rGO is confirmed by using FTIR, Raman spectroscopy, X-ray diffraction (XRD), etc. However, they have demonstrated that the GO to rGO can also be verified experimentally and theoretically by observing the shift in the resonance frequency, which forms the fundamental basis for 2D materials detections.

Furthermore, Hendry et al.[147] presented the plasmonic planar chiral metamaterials generated super chiral EM field that is very sensitive to the structure of chiral supramolecules. Also, they have reported that the effective refractive index variation of chiral samples exposed to left- and right-handed superchiral fields are 10^6 times larger than other optical polarimetry measurements, which allows the characterization of picogram quantities. Similarly, this chiral sensing approach is used further for detecting the interaction of antigen and antibody[148] and, most recently, the multiplexed biosensing for identifying the proteins and virions of SARS-CoV-2, Norovirus, and Zika virus.[149]

In addition to this, Yan et al.[150] demonstrated nanorod hyperbolic metamaterials and functionalized them with specific streptavidin immobilization, as shown in Figure 11(B). The sensorgram shows that the wavelength shifts depending on the concentration of streptavidin. Their reported sensitivity was 41,600 nm/RIU in the NIR region, and the detection limit was

https://doi.org/10.1021/acsomega.4c01872
ACS Omega 2024, 9, 24181−24202

0.14 μg/mL. Geng et al.[151] showcased the terahertz (THz) metamaterial with the microfluidic channel for liver cancer (glutamine transferase isozymes II (GGT-II) and alpha-fetoprotein (AFP)) bioassays detections using 19 and 14.2 GHz resonance wavelength shifts. Sreekanth et al.[152] proposed a hyperbolic metamaterial structure using Au/Al_2O_3 insulators and demonstrated the detection limit of a molecular weight up to 244 Da via streptavidin−biotin affinity interaction. Chen et al.[153] demonstrated the dual-band perfect absorber, achieving the maximum absorbance of 98% in two bands, as demonstrated in Figure 11(D), by breaking the cross-structural symmetry. Consequently, for two resonance bands, there are two different resonances of the electric field intensity, as well depicted in Figure 11(D) (iii−iv). Aksu et al.[154] presented the metasurface nanostructures on the flexible substrate for the first time fabricated using nano stencil lithography (NSL), which is capable of nanopatterning on the flexible substrate as shown in Figure 11(A) (v). This flexibility of metasurfaces is interesting because the optical responses can be turned mechanically based on substrate flexibility. Since metasurface performance also depends on the design approach, artificial intelligence (AI)[155] can be further implemented in the designing and data processing steps to design sensors with specific optical properties.

6. DEVELOPMENTS AND FUTURE PERSPECTIVES

The progression of material science and the accuracy of numerical analysis play vital roles in the recent development of optical biosensors. Simulation software such as COMSOL Multiphysics,[28,36] FDTD,[188,189] and CST[190] provides a closer look and helps to analyze experimental results for various geometrical and material parameters optimizations of biosensing platforms. Additionally, the combination of microfluidics[191,192] and, importantly, the most recent developments in flexible and stretchable[154] optical sensors have opened pathways to new functionalities and have become the most useable POC devices. The emphasis on POC devices for biosensing in healthcare and diagnostics has developed significantly in the last few decades.[193] One of the most challenging parts of developing POC devices is reducing the size without affecting the device's performance. Another one is the trade-off between the cost with respect to the detection accuracy of the POC biosensing devices. Developing a POC device that can detect molecular diagnosis with high accuracy and cost-effectiveness is difficult. Also, the accuracy of detection using the POC devices depends on the capability of handling the samples, so automated testing sample preparation is a prerequisite for working with consumers who are not experts in health care. Despite the challenges posed by the POC biosensors, several breakthroughs have been possible. For instance, the development of microfluidic technologies in fluidic engineering has given control over the flow in the micro- and nanoscale volumes.[194] Furthermore, wearable, flexible substrate-based POC biosensors have also gained increasing popularity. Moreover, the flexible substrate-based POC wearable devices with integrated graphene not only provide the continuous monitoring method in a noninvasive approach but also enhance the sensor sensitivity.[195] Finally, improved human device interfaces are becoming possible with the integration of AI for data analysis and accurate response in decision-making.

Each of the optical biosensors has its pros and cons in terms of operation and biosensing. However, compared to WGM and PhA optical biosensors, the research and development are currently more focused on plasmonics[95] and metasurface-based biosensing as they showcase high sensitivity and versatility. The flexibility and multifunctional materials have fueled recent research on the innovation of optical biosensors. Also, researchers are using the hybridization of the biosensors with various platforms to enhance their performance. Recently, emerging materials such as graphene,[196−198] transition metal dichalcogenide (TMDC),[199,200] and hybrid (graphene-TMDC)[201] have found their way into substantially developed ultrasensitive plasmonic biosensing compared to conventional bare metallic substrates. The reason behind the performance improvement with graphene and TMDC is that they contribute more electrons to transfer on the sensing surface to enhance the resonance oscillation that contributes to the efficiency of the sensor.

The emerging field of metasurfaces holds promise for LOC platforms and has garnered increased attention from optical biosensing research communities due to its versatility and high sensitivity. Nevertheless, several challenges persist,[18] including the absence of universal methods for large-scale metasurfaces fabrication, which currently relies on various laser direct write and nanoimprinting methods. Although metasurfaces report high sensitivities, their overall performance has not yet reached the levels achieved by plasmonic sensors. Furthermore, integrating plasmonic into systems containing microfluidics, complementary metal-oxide-semiconductor (CMOS) chips, and LOC devices is more mature, while dielectric metasurfaces are still in their infancy.

7. CONCLUSIVE REMARKS

This comprehensive review outlines various optical resonance biosensors, including WGM, PhA nanocavity, SPR, LSPR, and metasurfaces. Our discussion encompasses their structural design, sensing principles, the physics underlying their mechanisms, applications, current research progress, and their role in detecting diverse biomaterials. We initiated our review with the WGM microcavity, where the primary research focus centers on enhancing the quality factor to augment interactions with light and biomolecules. Subsequently, we delved into the PhA nanocavity, operating on PBG, and examined the development of nanocavities tailored to specific analyte sensing. After that, detailed insights into SPR and LSPR were provided, highlighting recent achievements in these sensing schemes as well as highlighted on SERS. We then shifted our focus to emerging metasurfaces, elucidating how they overcome the limitations of plasmonics and addressing associated challenges of their own. Additionally, we compiled a summary and tabulated the detailing of recent developments, minimum detection capabilities, and other characteristics of the bioassays for various optical biosensors, spanning from past to most recent developments in Table 1.

While these biosensors exhibit unique sensing mechanisms, further exploration is needed. In recent years, breakthroughs in different technological fields, such as microfabrication, electronics, physics, chemistry, biotechnology, and materials, have significantly advanced the fundamental understanding of optical biosensing. The gaps in multidimensional research focusing on specific applications are diminishing, which significantly accelerates biosensing research. Furthermore, early disease diagnosis is crucial for preventing widespread outbreaks, as evidenced by the recent COVID-19 pandemic. Plasmonics and metasurfaces-based biosensors are prevalent in

https://doi.org/10.1021/acsomega.4c01872
ACS Omega 2024, 9, 24181−24202

drug and vaccine research facilities. However, efforts are underway to make these biosensors more robust and reusable and integrate them into LOC systems to become mainstream in disease detection. Researchers are actively working on miniaturizing and compacting these optical biosensors into POC devices. One important point to note is that while maximizing sensitivity is a primary goal in developing biosensors, it is equally critical to balance cost-effectiveness, reusability, portability, and flexibility. This approach ensures the viability of these biosensors as POC platforms for medical applications, aiming to prevent and control potential outbreaks in the future.

AUTHOR INFORMATION

Corresponding Author

Kai Wu − *Department of Electrical and Computer Engineering, Texas Tech University, Lubbock, Texas 79409, United States;* orcid.org/0000-0002-9444-6112; Email: kai.wu@ttu.edu

Authors

Shahriar Mostufa − *Department of Electrical and Computer Engineering, Texas Tech University, Lubbock, Texas 79409, United States;* orcid.org/0000-0002-3326-4817

Bahareh Rezaei − *Department of Electrical and Computer Engineering, Texas Tech University, Lubbock, Texas 79409, United States*

Stefano Ciannella − *Department of Chemical Engineering, Texas Tech University, Lubbock, Texas 79409, United States*

Parsa Yari − *Department of Electrical and Computer Engineering, Texas Tech University, Lubbock, Texas 79409, United States*

Jenifer Gómez-Pastora − *Department of Chemical Engineering, Texas Tech University, Lubbock, Texas 79409, United States*

Rui He − *Department of Electrical and Computer Engineering, Texas Tech University, Lubbock, Texas 79409, United States;* orcid.org/0000-0002-2368-7269

Complete contact information is available at: https://pubs.acs.org/10.1021/acsomega.4c01872

Notes

The authors declare no competing financial interest.

ACKNOWLEDGMENTS

This study was financially supported by Texas Tech University through HEF New Faculty Startup, NRUF Start Up, and Core Research Support Fund. B. R. acknowledges the Distinguished Graduate Student Assistantships (DGSA) offered by Texas Tech University.

ABBREVIATIONS

(Ab)	Antibody
(AI)	Artificial Intelligence
(Au-FHA)	Gold Film Hemisphere Array
(AFP)	Alpha-fetoprotein
(CW)	Clockwise
(CCW)	Counterclockwise
(CEA)	Carcinoembryonic Antigen
(CMOS)	Complementary Metal Oxide Semiconductor
(DANG)	Dome Array with Nanogaps
(DHPE)	1,2-dihexadecanoyl-*sn*-glycero-3-phosphoethanolamine
(DOPC)	1,2-dioleoyl-*sn*-glycero-3-phosphocholine
(EM)	Electromagnetic
(ELISA)	Enzyme-Linked Immunosorbent Assays
(FDTD)	Finite Difference Time Domain
(FESEM)	Field Emission Scanning Electron Microscope
(FEM)	Finite Element Method
(GaHIgG)	Goat Anti-Human Immunoglobulin G
(GMR)	Giant Magnetic Resistance
(GGT-II)	Glutamine Transferase Isozymes II
(HIgG)	Human Immunoglobulin G
(InfA)	Influenza A virus
(LSPR)	Localized Surface Plasmon Resonance
(LOC)	Lab-on-Chip
(MgF_2)	Magnesium Fluoride
(ML)	Machine Learning
(MNP)	Magnetic Nanoparticles
(MoS_2)	Molybdenum Disulfide
(MTJ)	Magnetic Tunnel Junctions
(NHMMs)	Nanorod Hyperbolic Metamaterials
(OP)	Organophosphorus
(OSA)	Optical Spectrum Analyzer
(PCR)	Polymerase Chain Reaction
(PD)	Polarization Photodetector
(PDMS)	Polydimethylsiloxane
(PhA)	Photonic Crystal Array
(PBS)	Phosphate Buffered Saline
(PBG)	Photonic Band Gap
(PSA)	Prostate Specific Antigen
(PhA)	Photonic Crystal Array
(POC)	Point-of-Care
(r-GO)	Reduced Graphene Oxide
(SEMs)	Scanning Electrode Microscope
(SERS)	Surface Enhance Raman Scattering
(SOI)	Silicon on Insulator
(SPR)	Surface Plasmon Resonance
(SPW)	Surface Plasmon Waves
(SPP)	Surface Plasmon Polaritons
(TE)	Transverse Electric
(THz-TDS)	Terahertz Time-Domain Spectroscopy
(TIR)	Total Internal Reflection
(TM)	Transverse Magnetic
(TMDC)	Transition Metal Dichalcogenide
(VSV)	Vesicular Stomatitis Virus
(WGM)	Whispering Gallery Mode
(XRD)	X-ray diffraction

REFERENCES

(1) Zanchetta, G.; Lanfranco, R.; Giavazzi, F.; Bellini, T.; Buscaglia, M. Emerging Applications of Label-Free Optical Biosensors. *Nanophotonics* **2017**, *6* (4), 627−645.

(2) Chen, Y.; Liu, J.; Yang, Z.; Wilkinson, J. S.; Zhou, X. Optical Biosensors Based on Refractometric Sensing Schemes: A Review. *Biosens. Bioelectron.* **2019**, *144*, No. 111693.

(3) Damborský, P.; Švitel, J.; Katrlík, J. Optical Biosensors. *Essays Biochem.* **2016**, *60* (1), 91−100.

(4) Sadani, K.; Nag, P.; Mukherji, S. LSPR Based Optical Fiber Sensor with Chitosan Capped Gold Nanoparticles on BSA for Trace Detection of Hg (II) in Water, Soil and Food Samples. *Biosens. Bioelectron.* **2019**, *134*, 90−96.

(5) Akgönüllü, S.; Denizli, A. Recent Advances in Optical Biosensing Approaches for Biomarkers Detection. *Biosens. Bioelectron. X* **2022**, *12*, 100269.

https://doi.org/10.1021/acsomega.4c01872
ACS Omega 2024, 9, 24181−24202

(6) Ward, J.; Benson, O. WGM Microresonators: Sensing, Lasing and Fundamental Optics with Microspheres. *Laser Photonics Rev.* **2011**, *5* (4), 553−570.
(7) Yang, Y.; Wang, Z.; Zhang, X.; Zhang, Q.; Wang, T. *Recent Progress of In-Fiber WGM Microsphere Resonator*; Higher Education Press, 2023; Vol. *16*. DOI: 10.1007/s12200-023-00066-3.
(8) Chakravarty, S.; Chen, X.; Tang, N.; Lai, W. C.; Zou, Y.; Yan, H.; Chen, R. T. Review of Design Principles of 2D Photonic Crystal Microcavity Biosensors in Silicon and Their Applications. *Front. Optoelectron.* **2016**, *9* (2), 206−224.
(9) Shi, Q.; Zhao, J.; Liang, L. Two Dimensional Photonic Crystal Slab Biosensors Using Label Free Refractometric Sensing Schemes: A Review. *Prog. Quantum Electron.* **2021**, *77*, No. 100298.
(10) Syed Nor, S. N.; Rasanang, N. S.; Karman, S.; Zaman, W. S. W. K.; Harun, S. W.; Arof, H. A Review: Surface Plasmon Resonance-Based Biosensor for Early Screening of SARS-CoV2 Infection. *IEEE Access* **2022**, *10*, 1228−1244.
(11) Uniyal, S.; Choudhary, K.; Sachdev, S.; Kumar, S. Recent Advances in K-SPR Sensors for the Detection of Biomolecules and Microorganisms: A Review. *IEEE Sens. J.* **2022**, *22* (12), 11415−11426.
(12) Oh, S. H.; Altug, H. Performance Metrics and Enabling Technologies for Nanoplasmonic Biosensors. *Nat. Commun.* **2018**, *9* (1), 1−5.
(13) Altug, H.; Oh, S. H.; Maier, S. A.; Homola, J. Advances and Applications of Nanophotonic Biosensors. *Nat. Nanotechnol.* **2022**, *17* (1), 5−16.
(14) Lyu, D.; Huang, Q.; Wu, X.; Nie, Y.; Yang, M. Optical Fiber Sensors for Water and Air Quality Monitoring: A Review. *Opt. Eng.* **2024**, *63* (03). DOI: 10.1117/1.OE.63.3.031004.
(15) Paiva, J. S.; Jorge, P. A. S.; Rosa, C. C.; Cunha, J. P. S. Optical Fiber Tips for Biological Applications: From Light Confinement, Biosensing to Bioparticles Manipulation. *Biochim. Biophys. Acta - Gen. Subj.* **2018**, *1862* (5), 1209−1246.
(16) Zhang, T.; Zheng, Y.; Wang, C.; Mu, Z.; Liu, Y.; Lin, J. A Review of Photonic Crystal Fiber Sensor Applications for Different Physical Quantities. *Appl. Spectrosc. Rev.* **2018**, *53* (6), 486−502.
(17) Rifat, A. A.; Ahmed, R.; Yetisen, A. K.; Butt, H.; Sabouri, A.; Mahdiraji, G. A.; Yun, S. H.; Adikan, F. R. M. Photonic Crystal Fiber Based Plasmonic Sensors. *Sensors Actuators, B Chem.* **2017**, *243*, 311−325.
(18) Tseng, M. L.; Jahani, Y.; Leitis, A.; Altug, H. Dielectric Metasurfaces Enabling Advanced Optical Biosensors. *ACS Photonics* **2021**, *8* (1), 47−60.
(19) Qin, J.; Jiang, S.; Wang, Z.; Cheng, X.; Li, B.; Shi, Y.; Tsai, D. P.; Liu, A. Q.; Huang, W.; Zhu, W. Metasurface Micro/Nano-Optical Sensors: Principles and Applications. *ACS Nano* **2022**, *16* (8), 11598−11618.
(20) Wu, K.; Su, D.; Saha, R.; Wang, J. P. Giant Magnetoresistance (GMR) Materials and Devices for Biomedical and Industrial Applications. *Spintron. Mater. Devices, Appl.* **2022**, 3−49.
(21) Gawade, T. C.; Borole, U. P.; Behera, B.; Khan, J.; Barshilia, H. C.; Chowdhury, P. Giant Magnetoresistance (GMR) Spin-Valve Based Magnetic Sensor with Linear and Bipolar Characteristics for Low Current Detection. *J. Magn. Magn. Mater.* **2023**, *573*, No. 170679.
(22) Wu, K.; Tonini, D.; Liang, S.; Saha, R.; Chugh, V. K.; Wang, J. P. Giant Magnetoresistance Biosensors in Biomedical Applications. *ACS Appl. Mater. Interfaces* **2022**, *14* (8), 9945−9969.
(23) Mostufa, S.; Rezaei, B.; Yari, P.; Xu, K.; Gómez-Pastora, J.; Sun, J.; Shi, Z.; Wu, K. Giant Magnetoresistance Based Biosensors for Cancer Screening and Detection. *ACS Appl. Bio Mater.* **2023**, *6* (10), 4042−4059.
(24) Wibowo, N. A.; Riyanto, C. A.; Suharyadi, E.; Sabarman, H. Giant Magnetoresistance Sensor for Rapid and Simple Bovine Serum Albumin Assay with Ag-Functionalized Iron Oxide Nanoparticles Label. *IEEE Sens. J.* **2023**, *23* (9), 9204−9209.
(25) Lei, Z. Q.; Li, L.; Li, G. J.; Leung, C. W.; Shi, J.; Wong, C. M.; Lo, K. C.; Chan, W. K.; Mak, C. S. K.; Chan, S. B.; Chan, N. M. M.; Leung, C. H.; Lai, P. T.; Pong, P. W. T. Liver Cancer Immunoassay with Magnetic Nanoparticles and MgO-Based Magnetic Tunnel Junction Sensors. *J. Appl. Phys.* **2012**, *111* (7), 120−123.
(26) Sharma, P. P.; Albisetti, E.; Massetti, M.; Scolari, M.; La Torre, C.; Monticelli, M.; Leone, M.; Damin, F.; Gervasoni, G.; Ferrari, G.; Salice, F.; Cerquaglia, E.; Falduti, G.; Cretich, M.; Marchisio, E.; Chiari, M.; Sampietro, M.; Petti, D.; Bertacco, R. Integrated Platform for Detecting Pathogenic DNA via Magnetic Tunneling Junction-Based Biosensors. *Sensors Actuators, B Chem.* **2017**, *242*, 280−287.
(27) Luchansky, M. S.; Bailey, R. C. High- Q Optical Sensors for Chemical and Biological Analysis. *Anal. Chem.* **2012**, *84* (2), 793−821.
(28) Mostufa, S.; Akib, T. B. A.; Rana, M. M.; Islam, M. R. Highly Sensitive TiO2/Au/Graphene Layer-Based Surface Plasmon Resonance Biosensor for Cancer Detection. *Biosensors* **2022**, *12* (8), 603.
(29) Markoulatos, P.; Siafakas, N.; Moncany, M. Multiplex Polymerase Chain Reaction: A Practical Approach. *J. Clin. Lab. Anal.* **2002**, *16* (1), 47−51.
(30) Wilhelm, J.; Pingoud, A. Real-Time Polymerase Chain Reaction. *ChemBioChem.* **2003**, *4* (11), 1120−1128.
(31) Kubista, M.; Andrade, J. M.; Bengtsson, M.; Forootan, A.; Jonák, J.; Lind, K.; Sindelka, R.; Sjöback, R.; Sjögreen, B.; Strömbom, L.; Ståhlberg, A.; Zoric, N. The Real-Time Polymerase Chain Reaction. *Mol. Aspects Med.* **2006**, *27* (2−3), 95−125.
(32) Zhao, Q.; Lu, D.; Zhang, G.; Zhang, D.; Shi, X. Recent Improvements in Enzyme-Linked Immunosorbent Assays Based on Nanomaterials. *Talanta* **2021**, *223*, No. 121722.
(33) Gan, S. D.; Patel, K. R. Enzyme Immunoassay and Enzyme-Linked Immunosorbent Assay. *J. Invest. Dermatol.* **2013**, *133* (9), 1−3.
(34) Yanik, A. A.; Huang, M.; Kamohara, O.; Artar, A.; Geisbert, T. W.; Connor, J. H.; Altug, H. An Optofluidic Nanoplasmonic Biosensor for Direct Detection of Live Viruses from Biological Media. *Nano Lett.* **2010**, *10* (12), 4962−4969.
(35) Estevez, M. C.; Alvarez, M.; Lechuga, L. M. Integrated Optical Devices for Lab-on-a-Chip Biosensing Applications. *Laser and Photonics Reviews.* **2012**, *6*, 463−487.
(36) Mostufa, S.; Yari, P.; Rezaei, B.; Xu, K.; Sun, J.; Shi, Z.; Wu, K. Metamaterial as Perfect Absorber for High Sensitivity Refractive Index Based Biosensing Applications at Infrared Frequencies. *J. Phys. D. Appl. Phys.* **2023**, *56* (44), 445104.
(37) Karawdeniya, B. I.; Damry, A. M.; Murugappan, K.; Manjunath, S.; Bandara, Y. M. N. D. Y.; Jackson, C. J.; Tricoli, A.; Neshev, D. Surface Functionalization and Texturing of Optical Metasurfaces for Sensing Applications. *Chem. Rev.* **2022**, *122* (19), 14990−15030.
(38) Rho, D.; Breaux, C.; Kim, S. Label-Free Optical Resonator-Based Biosensors. *Sensors (Switzerland)* **2020**, *20* (20), 5901.
(39) Estevez, M. C.; Alvarez, M.; Lechuga, L. M. Integrated Optical Devices for Lab-on-a-Chip Biosensing Applications. *Laser Photon. Rev.* **2012**, *6* (4), 463−487.
(40) Su, J.; Goldberg, A. F. G.; Stoltz, B. M. Label-Free Detection of Single Nanoparticles and Biological Molecules Using Microtoroid Optical Resonators. *Light Sci. Appl.* **2016**, *5* (1), e16001−e16001.
(41) Shen, B.-Q.; Yu, X.-C.; Zhi, Y.; Wang, L.; Kim, D.; Gong, Q.; Xiao, Y.-F. Detection of Single Nanoparticles Using the Dissipative Interaction in a High-Q Microcavity. *Phys. Rev. Appl.* **2016**, *5* (2), 24011.
(42) Baaske, M. D.; Foreman, M. R.; Vollmer, F. Single-Molecule Nucleic Acid Interactions Monitored on a Label-Free Microcavity Biosensor Platform. *Nat. Nanotechnol.* **2014**, *9* (11), 933−939.
(43) Yang, G.; White, I. M.; Fan, X. An Opto-Fluidic Ring Resonator Biosensor for the Detection of Organophosphorus Pesticides. *Sensors Actuators, B Chem.* **2008**, *133* (1), 105−112.
(44) Lai, M.; Slaughter, G. Label-Free MicroRNA Optical Biosensors. *Nanomaterials* **2019**, *9* (11), 1573.
(45) Wong, L. S.; Khan, F.; Micklefield, J. Selective Covalent Protein Immobilization: Strategies and Applications. *Chem. Rev.* **2009**, *109* (9), 4025−4053.
(46) Khan, S.; Burciu, B.; Filipe, C. D. M.; Li, Y.; Dellinger, K.; Didar, T. F. DNAzyme-Based Biosensors: Immobilization Strategies,

Applications, and Future Prospective. *ACS Nano* **2021**, *15* (9), 13943−13969.
(47) Shen, Y.; Mackey, G.; Rupcich, N.; Gloster, D.; Chiuman, W.; Li, Y.; Brennan, J. D. Entrapment of Fluorescence Signaling DNA Enzymes in Sol-Gel-Derived Materials for Metal Ion Sensing. *Anal. Chem.* **2007**, *79* (9), 3494−3503.
(48) Swearingen, C. B.; Wernette, D. P.; Cropek, D. M.; Lu, Y.; Sweedler, J. V.; Bohn, P. W. Immobilization of a Catalytic DNA Molecular Beacon on Au for Pb(II) Detection. *Anal. Chem.* **2005**, *77* (2), 442−448.
(49) Nguyen, T. T.; Sly, K. L.; Conboy, J. C. Comparison of the Energetics of Avidin, Streptavidin, NeutrAvidin, and Anti-Biotin Antibody Binding to Biotinylated Lipid Bilayer Examined by Second-Harmonic Generation. *Anal. Chem.* **2012**, *84* (1), 201−208.
(50) Primiceri, E.; Chiriacò, M. S.; Notarangelo, F. M.; Crocamo, A.; Ardissino, D.; Cereda, M.; Bramanti, A. P.; Bianchessi, M. A.; Giannelli, G.; Maruccio, G. Key Enabling Technologies for Point-of-Care Diagnostics. *Sensors (Switzerland)* **2018**, *18* (11), 3607.
(51) Jokerst, J. V.; Jacobson, J. W.; Bhagwandin, B. D.; Floriano, P. N.; Christodoulides, N.; McDevitt, J. T. Programmable Nano-Bio-Chip Sensors: Analytical Meets Clinical. *Anal. Chem.* **2010**, *82* (5), 1571−1579.
(52) Ligler, F. S. Perspective on Optical Biosensors and Integrated Sensor Systems. *Anal. Chem.* **2009**, *81* (2), 519−526.
(53) Ozgur, E.; Toren, P.; Aktas, O.; Huseyinoglu, E.; Bayindir, M. Label-Free Biosensing with High Selectivity in Complex Media Using Microtoroidal Optical Resonators. *Sci. Rep.* **2015**, *5* (1), 9.
(54) Nur, S.; Lim, H. J.; Elzerman, J.; Morton, J. J. L. Silicon Photonic Crystal Cavities at near Band-Edge Wavelengths. *Appl. Phys. Lett.* **2019**, *114* (9), 1−5.
(55) Ouyang, Q.; Zeng, S.; Jiang, L.; Hong, L.; Xu, G.; Dinh, X. Q.; Qian, J.; He, S.; Qu, J.; Coquet, P.; Yong, K. T. Sensitivity Enhancement of Transition Metal Dichalcogenides/Silicon Nanostructure-Based Surface Plasmon Resonance Biosensor. *Sci. Rep.* **2016**, *6* (March), 1−13.
(56) Haider, F.; Ahmmed Aoni, R.; Ahmed, R.; Amouzad Mahdiraji, G.; Fahmi Azman, M.; Adikan, F. R. M. Mode-Multiplex Plasmonic Sensor for Multi-Analyte Detection. *Opt. Lett.* **2020**, *45* (14), 3945.
(57) Roh, S.; Chung, T.; Lee, B. Overview of the Characteristics of Micro- and Nano-Structured Surface Plasmon Resonance Sensors. *Sensors* **2011**, *11* (2), 1565−1588.
(58) Han, X. X.; Rodriguez, R. S.; Haynes, C. L.; Ozaki, Y.; Zhao, B. Surface-Enhanced Raman Spectroscopy. *Nat. Rev. Methods Prim.* **2021**, *1* (1), 87.
(59) Kim, K. H.; Jung, G. H.; Lee, S. J.; Park, H. G.; Park, Q. H. Ultrathin Capacitive Metasurfaces for Strong Electric Response. *Adv. Opt. Mater.* **2016**, *4* (10), 1501−1506.
(60) Foreman, M. R.; Swaim, J. D.; Vollmer, F. Whispering Gallery Mode Sensors: Erratum. *Adv. Opt. Photonics* **2015**, *7* (3), 632.
(61) Anwar, A. R.; Mur, M.; Humar, M. Microcavity- and Microlaser-Based Optical Barcoding: A Review of Encoding Techniques and Applications. *ACS Photonics* **2023**, *10* (5), 1202−1224.
(62) Loyez, M.; Adolphson, M.; Liao, J.; Yang, L. From Whispering Gallery Mode Resonators to Biochemical Sensors. *ACS Sensors* **2023**, *8* (7), 2440−2470.
(63) Vollmer, F.; Arnold, S.; Keng, D. Single Virus Detection from the Reactive Shift of a Whispering-Gallery Mode. *Proc. Natl. Acad. Sci. U. S. A.* **2008**, *105* (52), 20701−20704.
(64) Vollmer, F.; Arnold, S. Whispering-Gallery-Mode Biosensing: Label-Free Detection down to Single Molecules. *Nat. Methods* **2008**, *5* (7), 591−596.
(65) Quan, H.; Guo, Z. Simulation of Whispering-Gallery-Mode Resonance Shifts for Optical Miniature Biosensors. *J. Quant. Spectrosc. Radiat. Transfer* **2005**, *93* (1-3), 231−243.
(66) Baaske, M. D.; Foreman, M. R.; Vollmer, F. Single-Molecule Nucleic Acid Interactions Monitored on a Label-Free Microcavity Biosensor Platform. *Nat. Nanotechnol.* **2014**, *9* (11), 933−939.
(67) Subramanian, S.; Jones, H. B. L.; Frustaci, S.; Winter, S.; Van Der Kamp, M. W.; Arcus, V. L.; Pudney, C. R.; Vollmer, F. Sensing Enzyme Activation Heat Capacity at the Single-Molecule Level Using Gold-Nanorod-Based Optical Whispering Gallery Modes. *ACS Appl. Nano Mater.* **2021**, *4* (5), 4576.
(68) Zhu, J.; Ozdemir, S. K.; Xiao, Y. F.; Li, L.; He, L.; Chen, D. R.; Yang, L. On-Chip Single Nanoparticle Detection and Sizing by Mode Splitting in an Ultrahigh-Q Microresonator. *Nat. Photonics* **2010**, *4* (1), 46−49.
(69) Kim, W.; Özdemir, Ş. K.; Zhu, J.; Yang, L. Observation and Characterization of Mode Splitting in Microsphere Resonators in Aquatic Environment. *Appl. Phys. Lett.* **2011**, *98* (14), 2011−2014.
(70) Watts, A. L.; Singh, N.; Poulton, C. G.; Magi, E. C.; Kabakova, I. V.; Hudson, D. D.; Eggleton, B. J. Photoinduced Axial Quantization in Chalcogenide Microfiber Resonators. *J. Opt. Soc. Am. B* **2013**, *30* (12), 3249.
(71) Suresh, S.; Thomas, S. Comprehensive Review of Advances in the Field of Chalcogenide Glass Microresonators. *Int. J. Appl. Glas. Sci.* **2023**, *14* (2), 173−188.
(72) Duan, B.; Zou, H.; Chen, J.-H.; Ma, C. H.; Zhao, X.; Zheng, X.; Wang, C.; Liu, L.; Yang, D. High-Precision Whispering Gallery Microsensors with Ergodic Spectra Empowered by Machine Learning. *Photonics Res.* **2022**, *10* (10), 2343.
(73) Yablonovitch, E. Inhibited Spontaneous Emission in Solid-State Physics and Electronics. *Phys. Rev. Lett.* **1987**, *58* (20), 2059−2062.
(74) John, S. Strong Localization of Photons in Certain Disordered Dielectric Superlattices. *Phys. Rev. Lett.* **1987**, *58* (23), 2486−2489.
(75) Zhang, Y. N.; Zhao, Y.; Lv, R. Q. A Review for Optical Sensors Based on Photonic Crystal Cavities. *Sensors Actuators, A Phys.* **2015**, *233*, 374−389.
(76) Inan, H.; Poyraz, M.; Inci, F.; Lifson, M. A.; Baday, M.; Cunningham, B. T.; Demirci, U. Photonic Crystals: Emerging Biosensors and Their Promise for Point-of-Care Applications. *Chem. Soc. Rev.* **2017**, *46* (2), 366−388.
(77) Shi, Q.; Zhao, J.; Liang, L. Progress in Quantum Electronics Two Dimensional Photonic Crystal Slab Biosensors Using Label Free Refractometric Sensing Schemes : A Review. *Prog. Quantum Electron.* **2021**, *77*, No. 100298.
(78) Lee, M.; Fauchet, P. M. *Two-Dimensional Silicon Photonic Crystal Based Biosensing Platform for Protein Detection* **2007**, *15*, 4530−4535.
(79) Scullion, M. G.; Di Falco, A.; Krauss, T. F. Biosensors and Bioelectronics Slotted Photonic Crystal Cavities with Integrated Microfluidics for Biosensing Applications. *Biosens. Bioelectron.* **2011**, *27* (1), 101−105.
(80) Fan, X.; White, I. M.; Shopova, S. I.; Zhu, H.; Suter, J. D.; Sun, Y. Sensitive Optical Biosensors for Unlabeled Targets: A Review. *Anal. Chim. Acta* **2008**, *620* (1−2), 8−26.
(81) Zhang, Y.; Zhao, Y.; Zhou, T.; Wu, Q. Applications and Developments of On-Chip Biochemical Sensors Based on Optofluidic Photonic Crystal Cavities. *Lab Chip* **2018**, *18* (1), 57−74.
(82) Joannopoulos, J. D.; Villeneuve, P. R.; Fan, S. Photonic Crystals: Putting a New Twist on Light. *Nature* **1997**, *386* (6621), 143−149.
(83) Debnath, K.; Clementi, M.; Bucio, T. D.; Khokhar, A. Z.; Sotto, M.; Grabska, K. M.; Bajoni, D.; Galli, M.; Saito, S.; Gardes, F. Y. Ultrahigh-Q Photonic Crystal Cavities in Silicon Rich Nitride. *Opt. Express* **2017**, *25* (22), 27334.
(84) Liu, Y.; Zhang, X. Microfluidics-Based Plasmonic Biosensing System Based on Patterned Plasmonic Nanostructure Arrays. *Micromachines* **2021**, *12* (7), 826.
(85) Mostufa, S.; Paul, A. K.; Chakrabarti, K. Detection of Hemoglobin in Blood and Urine Glucose Level Samples Using a Graphene-Coated SPR Based Biosensor. *OSA Contin.* **2021**, *4* (8), 2164.
(86) Xu, Y.; Sun, M.; Wu, H.; Song, Y.; Wang, Q. Plasmonic Biosensor Based on Ag-TiO2-ZnO Gratings for Cancer Detection in the Optical Communication Band. *IEEE Sens. J.* **2023**, *23* (18), 20959−20967.

https://doi.org/10.1021/acsomega.4c01872
ACS Omega 2024, 9, 24181−24202

(87) Islam, M. R.; Jamil, M. A.; Zaman, M. S. U.; Ahsan, S. A. H.; Pulak, M. K.; Mehjabin, F.; Khan, M. M. I.; Chowdhury, J. A.; Islam, M. Design and Analysis of Birefringent SPR Based PCF Biosensor with Ultra-High Sensitivity and Low Loss. *Optik (Stuttg)* **2020**, *221* (July), No. 165311.
(88) Guo, X. Surface Plasmon Resonance Based Biosensor Technique: A Review. *J. Biophotonics* **2012**, *5* (7), 483−501.
(89) Konoplev, G.; Agafonova, D.; Bakhchova, L.; Mukhin, N.; Kurachkina, M.; Schmidt, M. P.; Verlov, N.; Sidorov, A.; Oseev, A.; Stepanova, O.; Kozyrev, A.; Dmitriev, A.; Hirsch, S. Label-Free Physical Techniques and Methodologies for Proteins Detection in Microfluidic Biosensor Structures. *Biomedicines* **2022**, *10* (2), 207.
(90) Iwata, T.; Mizutani, Y. Ellipsometric Measurement Technique for a Modified Otto Configuration Used for Observing Surface-Plasmon Resonance. *Opt. Express* **2010**, *18* (14), 14480.
(91) Steglich, P.; Lecci, G.; Mai, A. Surface Plasmon Resonance (SPR) Spectroscopy and Photonic Integrated Circuit (PIC) Biosensors: A Comparative Review. *Sensors* **2022**, *22* (8), 2901.
(92) Verma, A.; Sharma, A. K.; Prajapati, Y. K. On the Sensing Performance Enhancement in SPR-Based Biosensor Using Specific Two-Dimensional Materials (Borophene and Antimonene). *Opt. Mater. (Amst).* **2021**, *119* (July), No. 111355.
(93) Sathya, N.; Karki, B.; Rane, K. P.; Jha, A.; Pal, A. Tuning and Sensitivity Improvement of Bi-Metallic Structure-Based Surface Plasmon Resonance Biosensor with 2-D ϵ -Tin Selenide Nanosheets. *Plasmonics* **2022**, *17* (3), 1001−1008.
(94) Phan, Q. H.; Dinh, Q. T.; Pan, Y. C.; Huang, Y. T.; Hong, Z. H.; Lu, T. S. Decomposition Mueller Matrix Polarimetry for Enhanced MiRNA Detection with Antimonene-Based Surface Plasmon Resonance Sensor and DNA-Linked Gold Nanoparticle Signal Amplification. *Talanta* **2024**, *270*, No. 125611.
(95) Mahmud, R. Al; Sagor, R. H.; Khan, M. Z. M. Surface Plasmon Refractive Index Biosensors: A Review of Optical Fiber, Multilayer 2D Material and Gratings, and MIM Configurations. *Opt. Laser Technol.* **2023**, *159*, No. 108939.
(96) Kaushik, S.; Tiwari, U. K.; Pal, S. S.; Sinha, R. K. Rapid Detection of Escherichia Coli Using Fiber Optic Surface Plasmon Resonance Immunosensor Based on Biofunctionalized Molybdenum Disulfide (MoS_2) Nanosheets. *Biosens. Bioelectron.* **2019**, *126*, 501−509.
(97) Lang, T.; Cao, B.; Shen, C.; Shi, G. Multimode-Coreless-Multimode Fiber Biosensor Based on Surface Plasmon Resonance. *J. Phys. D. Appl. Phys.* **2019**, *52*, 195204.
(98) Kim, H.-M.; Lee, H.-Y.; Park, J.-H.; Lee, S.-K. Fiber Optic Plasmonic Sensors Based on Nanodome Arrays with Nanogaps. *ACS Sensors* **2022**, *7* (5), 1451−1457.
(99) Otupiri, R.; Akowuah, E. K.; Haxha, S. Multi-Channel SPR Biosensor Based on PCF for Multi-Analyte Sensing Applications. *Opt. Express* **2015**, *23* (12), 15716.
(100) Islam, M. R.; Hasan, K. R.; Khan, M. M. I.; Iftekher, A. N. M.; Mehjabin, F.; Nayen, M. J.; Chowdhury, J. A.; Islam, S. Bin; Islam, M. Design of a Dual Cluster and Dual Array-Based PCF-SPR Biosensor with Ultra-High WS and FOM. *Plasmonics* **2022**, *17* (3), 1171−1182.
(101) Chaudhary, V. S.; Kumar, D.; Kumar, S. Gold-Immobilized Photonic Crystal Fiber-Based SPR Biosensor for Detection of Malaria Disease in Human Body. *IEEE Sens. J.* **2021**, *21* (16), 17800−17807.
(102) Yu, R.; Chen, Y.; Shui, L.; Xiao, L. Hollow-Core Photonic Crystal Fiber Gas Sensing. *Sensors (Switzerland)* **2020**, *20* (10), 2996.
(103) Varshney, S. K.; Saitoh, K.; Saitoh, N.; Tsuchida, Y.; Koshiba, M.; Sinha, R. K. Strategies for Realizing Photonic Crystal Fiber Bandpass Filters. *Opt. Express* **2008**, *16* (13), 9459.
(104) Jollivet, C.; Guer, J.; Hofmann, P.; Schulzgen, A. Monolithic Fiber Lasers Combining Active PCF with Bragg Gratings in Conventional Single-Mode Fibers. *IEEE J. Sel. Top. Quantum Electron.* **2014**, *20* (5), 36.
(105) Hameed, M. F. O.; Heikal, A. M.; Younis, B. M.; Abdelrazzak, M.; Obayya, S. S. A. Ultra-High Tunable Liquid Crystal-Plasmonic Photonic Crystal Fiber Polarization Filter. *Opt. Express* **2015**, *23* (6), 7007.
(106) Jahan, N.; Rahman, M. M.; Ahsan, M.; Based, M. A.; Rana, M. M.; Gurusamy, S.; Haider, J. Photonic Crystal Fiber Based Biosensor for Pseudomonas Bacteria Detection: A Simulation Study. *IEEE Access* **2021**, *9*, 42206−42215.
(107) Ahmed, K.; Alzain, M. A.; Abdullah, H.; Luo, Y.; Vigneswaran, D.; Faragallah, O. S.; Eid, M. M. A.; Rashed, A. N. Z. Highly Sensitive Twin Resonance Coupling Refractive Index Sensor Based on Gold- and Mgf2-Coated Nano Metal Films. *Biosensors* **2021**, *11* (4), 104.
(108) Shakya, A. K.; Ramola, A.; Singh, S.; Van, V. Design of an Ultra-Sensitive Bimetallic Anisotropic PCF SPR Biosensor for Liquid Analytes Sensing. *Opt. Express* **2022**, *30* (6), 9233.
(109) Hu, D. J. J.; Ho, H. P. Recent Advances in Plasmonic Photonic Crystal Fibers: Design, Fabrication and Applications. *Adv. Opt. Photonics* **2017**, *9* (2), 257.
(110) Wu, T.; Shao, Y.; Wang, Y.; Cao, S.; Cao, W.; Zhang, F.; Liao, C.; He, J.; Huang, Y.; Hou, M.; Wang, Y. Surface Plasmon Resonance Biosensor Based on Gold-Coated Side-Polished Hexagonal Structure Photonic Crystal Fiber. *Opt. Express* **2017**, *25* (17), 20313.
(111) Paul, A. K.; Mollah, M. A.; Hassan, M. Z.; Gomez-Cardona, N.; Reyes-Vera, E. Graphene-Coated Highly Sensitive Photonic Crystal Fiber Surface Plasmon Resonance Sensor for Aqueous Solution: Design and Numerical Analysis. *Photonics* **2021**, *8* (5), 155.
(112) Belushkin, A.; Yesilkoy, F.; Altug, H. Nanoparticle-Enhanced Plasmonic Biosensor for Digital Biomarker Detection in a Microarray. *ACS Nano* **2018**, *12* (5), 4453−4461.
(113) Limaj, O.; Etezadi, D.; Wittenberg, N. J.; Rodrigo, D.; Yoo, D.; Oh, S. H.; Altug, H. Infrared Plasmonic Biosensor for Real-Time and Label-Free Monitoring of Lipid Membranes. *Nano Lett.* **2016**, *16* (2), 1502−1508.
(114) Etezadi, D.; Warner, J. B.; Lashuel, H. A.; Altug, H. Real-Time in Situ Secondary Structure Analysis of Protein Monolayer with Mid-Infrared Plasmonic Nanoantennas. *ACS Sensors* **2018**, *3* (6), 1109−1117.
(115) Adato, R.; Yanik, A. A.; Amsden, J. J.; Kaplan, D. L.; Omenetto, F. G.; Hong, M. K.; Erramilli, S.; Altug, H. Ultra-Sensitive Vibrational Spectroscopy of Protein Monolayers with Plasmonic Nanoantenna Arrays. *Proc. Natl. Acad. Sci. U. S. A.* **2009**, *106* (46), 19227−19232.
(116) Yanik, A. A.; Cetin, A. E.; Huang, M.; Artar, A.; Mousavi, S. H.; Khanikaev, A.; Connor, J. H.; Shvets, G.; Altug, H. Seeing Protein Monolayers with Naked Eye through Plasmonic Fano Resonances. *Proc. Natl. Acad. Sci. U. S. A.* **2011**, *108* (29), 11784−11789.
(117) Hao, F.; Nordlander, P.; Sonnefraud, Y.; Van Dorpe, P.; Maier, S. A. Tunability of Subradiant Dipolar and Fano-Type Plasmon Resonances in Metallic Ring/Disk Cavities: Implications for Nano-scale Optical Sensing. *ACS Nano* **2009**, *3* (3), 643−652.
(118) Cetin, A. E.; Coskun, A. F.; Galarreta, B. C.; Huang, M.; Herman, D.; Ozcan, A.; Altug, H. Handheld High-Throughput Plasmonic Biosensor Using Computational on-Chip Imaging. *Light Sci. Appl.* **2014**, *3* (1), e122.
(119) Li, X.; Soler, M.; Özdemir, C. I.; Belushkin, A.; Yesilköy, F.; Altug, H. Plasmonic Nanohole Array Biosensor for Label-Free and Real-Time Analysis of Live Cell Secretion. *Lab Chip* **2017**, *17* (13), 2208−2217.
(120) Rodrigo, D.; Limaj, O.; Janner, D.; Etezadi, D.; García de Abajo, F. J.; Pruneri, V.; Altug, H. Mid-Infrared Plasmonic Biosensing with Graphene. *Science (80-.)* **2015**, *349* (6244), 165−168.
(121) Zijlstra, P.; Paulo, P. M. R.; Orrit, M. Optical Detection of Single Non-Absorbing Molecules Using the Surface Plasmon Resonance of a Gold Nanorod. *Nat. Nanotechnol.* **2012**, *7* (6), 379−382.
(122) Fleischmann, M.; Hendra, P. J.; McQuillan, A. J. Raman Spectra of Pyridine Adsorbed at a Silver Electrode. *Chem. Phys. Lett.* **1974**, *26* (2), 163−166.
(123) Shu, L.; Zhou, J.; Yuan, X.; Petti, L.; Chen, J.; Jia, Z.; Mormile, P. Highly Sensitive Immunoassay Based on SERS Using Nano-Au Immune Probes and a Nano-Ag Immune Substrate. *Talanta* **2014**, *123*, 161−168.

https://doi.org/10.1021/acsomega.4c01872
ACS Omega 2024, 9, 24181−24202

(124) Palermo, G.; Rippa, M.; Conti, Y.; Vestri, A.; Castagna, R.; Fusco, G.; Suffredini, E.; Zhou, J.; Zyss, J.; De Luca, A.; Petti, L. Plasmonic Metasurfaces Based on Pyramidal Nanoholes for High-Efficiency SERS Biosensing. *ACS Appl. Mater. Interfaces* **2021**, *13* (36), 43715−43725.
(125) Peng, L.; Zhou, J.; Liang, Z.; Zhang, Y.; Petti, L.; Jiang, T.; Gu, C.; Yang, D.; Mormile, P. SERS-Based Sandwich Bioassay Protocol of MiRNA-21 Using Au@Ag Core-Shell Nanoparticles and a Ag/TiO_2 Nanowires Substrate. *Anal. Methods* **2019**, *11* (23), 2960−2968.
(126) Rippa, M.; Sagnelli, D.; Vestri, A.; Marchesano, V.; Munari, B.; Carnicelli, D.; Varrone, E.; Brigotti, M.; Tozzoli, R.; Montalbano, M.; Morabito, S.; Zhou, J.; Zyss, J.; Petti, L. Plasmonic Metasurfaces for Specific SERS Detection of Shiga Toxins. *ACS Appl. Mater. Interfaces* **2022**, *14* (4), 4969−4979.
(127) Wang, Z.; Yang, H.; Wang, M.; Petti, L.; Jiang, T.; Jia, Z.; Xie, S.; Zhou, J. SERS-Based Multiplex Immunoassay of Tumor Markers Using Double SiO2@Ag Immune Probes and Gold-Film Hemisphere Array Immune Substrate. *Colloids Surfaces A Physicochem. Eng. Asp.* **2018**, *546*, 48−58.
(128) Xu, W.; Xie, L.; Ying, Y. Mechanisms and Applications of Terahertz Metamaterial Sensing: A Review. *Nanoscale* **2017**, *9*, 13864−13878.
(129) Fan, S.; Davies Wykes, M.S.; Lin, W.E.; Jones, R.L.; Robins, A.G.; Linden, P.F. A full-scale field study for evaluation of simple analytical models of cross ventilation and single-sided ventilation. *Build. Environ* **2021**, *187*, No. 107386.
(130) Liu, W.; Li, Z.; Cheng, H.; Chen, S. Dielectric Resonance-Based Optical Metasurfaces: From Fundamentals to Applications. *iScience* **2020**, *23* (12), No. 101868.
(131) Kruk, S.; Kivshar, Y. Functional Meta-Optics and Nanophotonics Govern by Mie Resonances. *ACS Photonics* **2017**, *4* (11), 2638−2649.
(132) Xin, W.; Binzhen, Z.; Wanjun, W.; Junlin, W.; Junping, D. Design, Fabrication, and Characterization of a Flexible Dual-Band Metamaterial Absorber. *IEEE Photonics J.* **2017**, *9* (4), 1.
(133) Bi, H.; You, R.; Bian, X.; Li, P.; Zhao, X.; You, Z. A Magnetic Control Enrichment Technique Combined with Terahertz Metamaterial Biosensor for Detecting SARS-CoV-2 Spike Protein. *Biosens. Bioelectron.* **2024**, *243*, No. 115763.
(134) Ray, D.; Raziman, T. V.; Santschi, C.; Etezadi, D.; Altug, H.; Martin, O. J. F. Hybrid Metal-Dielectric Metasurfaces for Refractive Index Sensing. *Nano Lett.* **2020**, *20* (12), 8752−8759.
(135) O'Hara, J. F.; Singh, R.; Brener, I.; Smirnova, E.; Han, J.; Taylor, A. J.; Zhang, W. Thin-Film Sensing with Planar Terahertz Metamaterials: Sensitivity and Limitations. *Opt. Express* **2008**, *16* (3), 1786.
(136) Singh, R.; Rockstuhl, C.; Lederer, F.; Zhang, W. The Impact of Nearest Neighbor Interaction on the Resonances in Terahertz Metamaterials. *Appl. Phys. Lett.* **2009**, *94* (2). DOI: 10.1063/1.3063051.
(137) Chiam, S. Y.; Singh, R.; Zhang, W.; Bettiol, A. A. Controlling Metamaterial Resonances via Dielectric and Aspect Ratio Effects. *Appl. Phys. Lett.* **2010**, *97* (19), 9−12.
(138) Gu, J.; Han, J.; Lu, X.; Singh, R.; Tian, Z.; Xing, Q.; Zhang, W. A Close-Ring Pair Terahertz Metamaterial Resonating at Normal Incidence. *Opt. Express* **2009**, *17* (22), 20307.
(139) Tian, Z.; Singh, R.; Han, J.; Gu, J.; Xing, Q.; Wu, J.; Zhang, W. Terahertz Superconducting Plasmonic Hole Array. *Opt. Lett.* **2010**, *35* (21), 3586.
(140) Saleh, G.; Ateeq, I. S.; Al-Naib, I. Glucose Level Sensing Using Single Asymmetric Split Ring Resonator. *Sensors* **2021**, *21* (9), 2945.
(141) Chen, M.; Singh, L.; Xu, N.; Singh, R.; Zhang, W.; Xie, L. Terahertz Sensing of Highly Absorptive Water-Methanol Mixtures with Multiple Resonances in Metamaterials. *Opt. Express* **2017**, *25* (13), 14089.
(142) Xu, J.; Liao, D.; Gupta, M.; Zhu, Y.; Zhuang, S.; Singh, R.; Chen, L. Terahertz Microfluidic Sensing with Dual-Torus Toroidal Metasurfaces. *Adv. Opt. Mater.* **2021**, *9* (15), 1−8.
(143) Sreekanth, K. V.; Mahalakshmi, P.; Han, S.; Mani Rajan, M. S.; Choudhury, P. K.; Singh, R. Brewster Mode-Enhanced Sensing with Hyperbolic Metamaterial. *Adv. Opt. Mater.* **2019**, *7* (21), 1−6.
(144) Gupta, M.; Singh, R. Terahertz Sensing with Optimized Q/Veff Metasurface Cavities. *Adv. Opt. Mater.* **2020**, *8* (16), 1−7.
(145) Lim, W. X.; Manjappa, M.; Pitchappa, P.; Singh, R. Shaping High-Q Planar Fano Resonant Metamaterials toward Futuristic Technologies. *Adv. Opt. Mater.* **2018**, *6* (19). DOI: 10.1002/adom.201800502.
(146) Sajeev, V.; Rane, S.; Ghosh, D.; Acharyya, N.; Roy Choudhury, P.; Mukherjee, A.; Roy Chowdhury, D. Terahertz Sensing of Reduced Graphene Oxide Nanosheets Using Sub-Wavelength Dipole Cavities. *Sci. Rep.* **2023**, *13* (1), 1−9.
(147) Hendry, E.; Carpy, T.; Johnston, J.; Popland, M.; Mikhaylovskiy, R. V.; Lapthorn, A. J.; Kelly, S. M.; Barron, L. D.; Gadegaard, N.; Kadodwala, M. Ultrasensitive Detection and Characterization of Biomolecules Using Superchiral Fields. *Nat. Nanotechnol.* **2010**, *5* (11), 783−787.
(148) Koyroytsaltis-McQuire, D. J. P.; Gilroy, C.; Barron, L. D.; Gadegaard, N.; Karimullah, A. S.; Kadodwala, M. Detecting Antibody−Antigen Interactions with Chiral Plasmons: Factors Influencing Chiral Plasmonic Sensing. *Adv. Photonics Res.* **2022**, *3* (1), 1−12.
(149) Wallace, S.; Kartau, M.; Kakkar, T.; Davis, C.; Szemiel, A.; Samardzhieva, I.; Vijayakrishnan, S.; Cole, S.; De Lorenzo, G.; Maillart, E.; Gautier, K.; Lapthorn, A. J.; Patel, A. H.; Gadegaard, N.; Kadodwala, M.; Hutchinson, E.; Karimullah, A. S. Multiplexed Biosensing of Proteins and Virions with Disposable Plasmonic Assays. *ACS Sensors* **2023**, *8* (9), 3338−3348.
(150) Yan, R.; Wang, T.; Yue, X.; Wang, H.; Zhang, Y.-H.; Xu, P.; Wang, L.; Wang, Y.; Zhang, J. Highly Sensitive Plasmonic Nanorod Hyperbolic Metamaterial Biosensor. *Photonics Res.* **2022**, *10* (1), 84.
(151) Geng, Z.; Zhang, X.; Fan, Z.; Lv, X.; Chen, H. A Route to Terahertz Metamaterial Biosensor Integrated with Microfluidics for Liver Cancer Biomarker Testing in Early Stage. *Sci. Rep.* **2017**, *7* (1), 1−11.
(152) Sreekanth, K. V.; Alapan, Y.; Elkabbash, M.; Ilker, E.; Hinczewski, M.; Gurkan, U. A.; De Luca, A.; Strangi, G. Extreme Sensitivity Biosensing Platform Based on Hyperbolic Metamaterials. *Nat. Mater.* **2016**, *15* (6), 621−627.
(153) Chen, K.; Adato, R.; Altug, H. Dual-Band Perfect Absorber for Multispectral Plasmon-Enhanced Infrared Spectroscopy. *ACS Nano* **2012**, *6* (9), 7998−8006.
(154) Aksu, S.; Huang, M.; Artar, A.; Yanik, A. A.; Selvarasah, S.; Dokmeci, M. R.; Altug, H. Flexible Plasmonics on Unconventional and Nonplanar Substrates. *Adv. Mater.* **2011**, *23* (38), 4422−4430.
(155) Malkiel, I.; Mrejen, M.; Nagler, A.; Arieli, U.; Wolf, L.; Suchowski, H. Plasmonic Nanostructure Design and Characterization via Deep Learning. *Light Sci. Appl.* **2018**, *7* (1). DOI: 10.1038/s41377-018-0060-7.
(156) Brice, I.; Grundsteins, K.; Atvars, A.; Alnis, J.; Viter, R.; Ramanavicius, A. Whispering Gallery Mode Resonator and Glucose Oxidase Based Glucose Biosensor. *Sensors Actuators, B Chem.* **2020**, *318*, No. 128004.
(157) Ouyang, X.; Liu, T.; Zhang, Y.; He, J.; He, Z.; Zhang, A. P.; Tam, H. Y. Ultrasensitive Optofluidic Enzyme-Linked Immunosorbent Assay by on-Chip Integrated Polymer Whispering-Gallery-Mode Microlaser Sensors. *Lab Chip* **2020**, *20* (14), 2438−2446.
(158) Hsieh, S. T.; Cheeney, J. E.; Ding, X.; Myung, N. V.; Haberer, E. D. Near-Field Electrospinning of Polymer/Phage Whispering Gallery Mode Microfiber Resonators for Label-Free Biosensing. *Sensors Actuators B Chem.* **2022**, *367* (April), No. 132062.
(159) Wan, H.; Zhang, S.; Gu, Y.; Xiong, J.; Xu, J.; Wan, C.; Chao, J. Label-Free, Ultra-Low Detection Limit DNA Biosensor Using High Quality Optical Microcavity Functionalized by DNA Tetrahedral Nanostructure Probes. *Nanophotonics* **2023**, *12* (16), 3323−3331.
(160) Sun, J.; Mao, W.; Xia, C.; Wang, W.; Cui, Q.; Shi, Z.; Zhu, G.; Wang, M.; Xu, C. Plasmon-Coupled GaN Microcavity for WGM

Lasing and Label-Free SERS Sensing of Biofluids. *Adv. Opt. Mater.* **2024**, DOI: 10.1002/adom.202301989.
(161) AbdelMalek, F. Design of a Novel Left-Handed Photonic Crystal Sensor Operating in Aqueous Environment. *IEEE Photonics Technol. Lett.* **2011**, *23* (3), 188−190.
(162) Pal, S.; Guillermain, E.; Sriram, R.; Miller, B. L.; Fauchet, P. M. Silicon Photonic Crystal Nanocavity-Coupled Waveguides for Error-Corrected Optical Biosensing. *Biosens. Bioelectron.* **2011**, *26* (10), 4024−4031.
(163) Wang, C.; Quan, Q.; Kita, S.; Li, Y.; Lončar, M. Single-Nanoparticle Detection with Slot-Mode Photonic Crystal Cavities. *Appl. Phys. Lett.* **2015**, *106* (26). DOI: 10.1063/1.4923322.
(164) Chen, Y. T.; Liao, Y. Y.; Chen, C. C.; Hsiao, H. H.; Huang, J. J. Surface Plasmons Coupled Two-Dimensional Photonic Crystal Biosensors for Epstein-Barr Virus Protein Detection. *Sensors Actuators, B Chem.* **2019**, *291*, 81−88.
(165) Baraty, F.; Hamedi, S. Label-Free Cancer Cell Biosensor Based on Photonic Crystal Ring Resonator. *Results Phys.* **2023**, *46*, No. 106317.
(166) Yadav, A.; Kumar, A.; Sharan, P.; Mishra, M. Highly Sensitive Bimetallic-Metal Nitride SPR Biosensor for Urine Glucose Detection. *IEEE Trans. Nanobioscience* **2023**, *22* (4), 897−903.
(167) Sayed, F. A.; Elsayed, H. A.; Al-Dossari, M.; Eissa, M. F.; Mehaney, A.; Aly, A. H. Angular Surface Plasmon Resonance-Based Sensor with a Silver Nanocomposite Layer for Effective Water Pollution Detection. *Sci. Rep.* **2023**, *13* (1), 1−19.
(168) Guner, H.; Ozgur, E.; Kokturk, G.; Celik, M.; Esen, E.; Topal, A. E.; Ayas, S.; Uludag, Y.; Elbuken, C.; Dana, A. Sensors and Actuators B : Chemical A Smartphone Based Surface Plasmon Resonance Imaging (SPRi) Platform for on-Site Biodetection. *Sensors Actuators B. Chem.* **2017**, *239*, 571−577.
(169) Chamoli, S. K.; Singh, S. C.; Guo, C. Design of Extremely Sensitive Refractive Index Sensors in Infrared for Blood Glucose Detection. *IEEE Sens. J.* **2020**, *20* (9), 4628−4634.
(170) Long, S.; Wang, E.; Wu, M.; Zhu, H.; Xu, N.; Wang, Y.; Cao, J. Sensors and Actuators : A. Physical Sensing Absorptive Fluids with Backside Illuminated Grating Coupled SPR Sensor Fabricated by Nanoimprint Technology. *Sensors Actuators A. Phys.* **2022**, *337*, No. 113416.
(171) Dong, J.; Zhang, Y.; Wang, Y.; Yang, F.; Hu, S.; Chen, Y.; Zhu, W.; Qiu, W.; Guan, H.; Lu, H.; Yu, J.; Zhong, Y.; Zhang, J.; Luo, Y.; Chen, Z. Side-Polished Few-Mode Fiber Based Surface Plasmon Resonance Biosensor. *Opt. Express* **2019**, *27* (8), 11348.
(172) Bahador, H.; Heidarzadeh, H. Analysis and Simulation of a Novel Localized Surface Plasmonic Highly Sensitive Refractive Index Sensor. *Plasmonics* **2020**, *15* (5), 1273−1279.
(173) Haider, F.; Ahmmed Aoni, R.; Ahmed, R.; Jen Chew, W.; Amouzad Mahdiraji, G. Plasmonic Micro-Channel Based Highly Sensitive Biosensor in Visible to Mid-IR. *Opt. Laser Technol.* **2021**, *140*, No. 107020.
(174) Kumar, A.; Verma, P.; Jindal, P. Surface Plasmon Resonance Biosensor Based on a D-Shaped Photonic Crystal Fiber Using Ti3C2Tx MXene Material. *Opt. Mater. (Amst).* **2022**, *128*, No. 112397.
(175) Xu-et-Al-2018-ω-Shaped-Fiber-Optic-Probe-Based-Localized-Surface-Plasmon-Resonance-Biosensor-for-Real-Time-Detection-of.Pdf.
(176) Li, L.; Zhang, Y.-n.; Zheng, W.; Li, X.; Zhao, Y. Optical Fiber SPR Biosensor Based on Gold Nanoparticle Amplification for DNA Hybridization Detection. *Talanta* **2022**, *247* (March), No. 123599.
(177) Wang, Y.; Singh, R.; Chaudhary, S.; Zhang, B.; Kumar, S. 2-D Nanomaterials Assisted LSPR MPM Optical Fiber Sensor Probe for Cardiac Troponin I Detection. *IEEE Trans. Instrum. Meas.* **2022**, *71*, 1−9.
(178) Bekmurzayeva, A.; Ashikbayeva, Z.; Assylbekova, N.; Myrkhiyeva, Z.; Dauletova, A.; Ayupova, T.; Shaimerdenova, M.; Tosi, D. Ultra-Wide, Attomolar-Level Limit Detection of CD44 Biomarker with a Silanized Optical Fiber Biosensor. *Biosens. Bioelectron.* **2022**, *208* (March), No. 114217.
(179) Lobry, M.; Loyez, M.; Debliquy, M.; Chah, K.; Goormaghtigh, E.; Caucheteur, C. Electro-Plasmonic-Assisted Biosensing of Proteins and Cells at the Surface of Optical Fiber. *Biosens. Bioelectron.* **2023**, *220*, 114867.
(180) Zhang, Y.; Ding, L.; Wang, S.; Jiang, X.; Ma, F.; Zhao, J.; Meng, W.; Gao, L. A New Acetylcholine Optical Fiber Biosensor Based on Gold Film-GNRs Resonance Coupling Enhancement. *IEEE Sens. J.* **2024**, *24*, 4557.
(181) Yesilkoy, F.; Arvelo, E. R.; Jahani, Y.; Liu, M.; Tittl, A.; Cevher, V.; Kivshar, Y.; Altug, H. Ultrasensitive Hyperspectral Imaging and Biodetection Enabled by Dielectric Metasurfaces. *Nat. Photonics* **2019**, *13* (6), 390−396.
(182) Bian, J.; Xing, X.; Zhou, S.; Man, Z.; Lu, Z.; Zhang, W. Patterned Plasmonic Gradient for High-Precision Biosensing Using a Smartphone Reader. *Nanoscale* **2019**, *11* (26), 12471−12476.
(183) Miao, X.; Yan, L.; Wu, Y.; Liu, P. Q. High-Sensitivity Nanophotonic Sensors with Passive Trapping of Analyte Molecules in Hot Spots. *Light Sci. Appl.* **2021**, *10* (1). DOI: 10.1038/s41377-020-00449-7.
(184) Jahani, Y.; Arvelo, E. R.; Yesilkoy, F.; Koshelev, K.; Cianciaruso, C.; De Palma, M.; Kivshar, Y.; Altug, H. Imaging-Based Spectrometer-Less Optofluidic Biosensors Based on Dielectric Metasurfaces for Detecting Extracellular Vesicles. *Nat. Commun.* **2021**, *12* (1), 4−13.
(185) Lin, S.; Xu, X.; Hu, F.; Chen, Z.; Wang, Y.; Zhang, L.; Peng, Z.; Li, D.; Zeng, L.; Chen, Y.; Wang, Z. Using Antibody Modified Terahertz Metamaterial Biosensor to Detect Concentration of Carcinoembryonic Antigen. *IEEE J. Sel. Top. Quantum Electron.* **2021**, *27* (4), 1.
(186) Lin, S.; Wang, Y.; Peng, Z.; Chen, Z.; Hu, F. Detection of Cancer Biomarkers CA125 and CA199 via Terahertz Metasurface Immunosensor. *Talanta* **2022**, *248*, No. 123628.
(187) Chen, J.; Hu, F.; Lin, S.; Song, Z.; Duan, Z.; Zhang, L.; Jiang, M. Hybridization Chain Reaction Assisted Terahertz Metamaterial Biosensor for Highly Sensitive Detection of MicroRNAs. *Spectrochim. Acta Part A Mol. Biomol. Spectrosc.* **2024**, *307*, No. 123646.
(188) Akib, T. B. A.; Mostufa, S.; Rana, M. M.; Hossain, M. B.; Islam, M. R. A Performance Comparison of Heterostructure Surface Plasmon Resonance Biosensor for the Diagnosis of Novel Coronavirus SARS-CoV-2. *Opt. Quantum Electron.* **2023**, *55* (5), 448.
(189) Yari, P.; Farmani, H.; Farmani, A. Steering of Guided Light with Graphene Metasurface for Refractive Index Sensing with High Figure of Merits. *Plasmonics* **2022**, *17* (1), 305−314.
(190) Chen, T.; Jiang, W.; Yin, X. Dual-Band Ultrasensitive Terahertz Sensor Based on Tunable Graphene Metamaterial Absorber. *Superlattices Microstruct.* **2021**, *154* (April), No. 106898.
(191) Hajba, L.; Guttman, A. Circulating Tumor-Cell Detection and Capture Using Microfluidic Devices. *TrAC - Trends Anal. Chem.* **2014**, *59*, 9−16.
(192) Yang, Z.; Xia, L.; Li, S.; Qi, R.; Chen, X.; Li, W. Highly Sensitive Refractive Index Detection Based on Compact HSC-SPR Structure in a Microfluidic Chip. *Sensors Actuators, A Phys.* **2019**, *297*, No. 111558.
(193) Rasheed, S.; Kanwal, T.; Ahmad, N.; Fatima, B.; Najam-ul-Haq, M.; Hussain, D. Advances and Challenges in Portable Optical Biosensors for Onsite Detection and Point-of-Care Diagnostics. *TrAC - Trends Anal. Chem.* **2024**, *173*, No. 117640.
(194) Wang, J.; Maier, S. A.; Tittl, A. Trends in Nanophotonics-Enabled Optofluidic Biosensors. *Adv. Opt. Mater.* **2022**, *10* (7). DOI: 10.1002/adom.202102366.
(195) Wang, S. Q.; Chinnasamy, T.; Lifson, M. A.; Inci, F.; Demirci, U. Flexible Substrate-Based Devices for Point-of-Care Diagnostics. *Trends Biotechnol.* **2016**, *34* (11), 909−921.
(196) Nurrohman, D. T.; Chiu, N. F. A Review of Graphene-Based Surface Plasmon Resonance and Surface-Enhanced Raman Scattering Biosensors: Current Status and Future Prospects. *Nanomaterials* **2021**, *11*, 216.
(197) Song, B.; Li, D.; Qi, W.; Elstner, M.; Fan, C.; Fang, H. Graphene on Au(111): A Highly Conductive Material with Excellent

Adsorption Properties for High-Resolution Bio/Nanodetection and Identification. *ChemPhysChem* **2010**, *11* (3), 585−589.
(198) Bi, H.; Yang, M.; You, R. Advances in Terahertz Metasurface Graphene for Biosensing and Application. *Discovery Nano* **2023**, *18* (1). DOI: 10.1186/s11671-023-03814-8.
(199) Wu, L.; Guo, J.; Wang, Q.; Lu, S.; Dai, X.; Xiang, Y.; Fan, D. Sensitivity Enhancement by Using Few-Layer Black Phosphorus-Graphene/TMDCs Heterostructure in Surface Plasmon Resonance Biochemical Sensor. *Sensors Actuators, B Chem.* **2017**, *249*, 542−548.
(200) Han, L.; He, X.; Ge, L.; Huang, T.; Ding, H.; Wu, C. Comprehensive Study of SPR Biosensor Performance Based on Metal-ITO-Graphene/TMDC Hybrid Multilayer. *Plasmonics* **2019**, *14* (6), 2021−2030.
(201) Jiang, L.; Zeng, S.; Ouyang, Q.; Dinh, X. Q.; Coquet, P.; Qu, J.; He, S.; Yong, K. T. Graphene-TMDC-Graphene Hybrid Plasmonic Metasurface for Enhanced Biosensing: A Theoretical Analysis. *Phys. Status Solidi Appl. Mater. Sci.* **2017**, *214* (12), 1−11.

https://doi.org/10.1021/acsomega.4c01872
ACS Omega 2024, 9, 24181−24202